Progress in Oceanography 209 (2022) 102904

Contents lists available at ScienceDirect

Progress in Oceanography

journal homepage: www.elsevier.com/locate/pocean

Unveiling deep-sea habitats of the Southern Ocean-facing submarine canyons of southwestern Australia

Julie A Trotter [a,*], Marco Taviani [b,c,d], Federica Foglini [b], Aleksey Sadekov [a], Grzegorz Skrzypek [e], Claudio Mazzoli [f], Alessandro Remia [b], Nadia Santodomingo [g], Giorgio Castellan [b], Malcolm McCulloch [a,h], Charitha Pattiaratchi [a], Paolo Montagna [i]

[a] Oceans Graduate School and UWA Oceans Institute, The University of Western Australia, Perth 6009, Australia
[b] Istituto di Scienze Marine (ISMAR), Consiglio Nazionale delle Ricerche (CNR), Bologna, Italy
[c] Stazione Zoologica Anton Dohrn, Naples, Italy
[d] Biology Department, Woods Hole Oceanographic Institution, Woods Hole, MA 02543, USA
[e] School of Biological Sciences, The University of Western Australia, Perth 6009, Australia
[f] Department of Geosciences, University of Padova, Padova 35131, Italy
[g] Department of Earth Sciences, Natural History Museum, Cromwell Road, SW7 5BD London, UK
[h] ARC Centre of Excellence in Coral Reef Studies, The University of Western Australia, Perth 6009, Australia
[i] Istituto di Scienze Polari (ISP), Consiglio Nazionale delle Ricerche (CNR), Bologna, Italy

ARTICLE INFO

Keywords:
Australian submarine canyons
Deep-water fauna
Remotely Operated Vehicle
Oceanography
Southern Ocean
Deep-water corals

ABSTRACT

Here we present the outcomes of the first deep-sea remotely operated vehicle study of previously unexplored submarine canyon systems along the southwest Australian continental margin. This was conducted around: (1) the Bremer Marine Park; (2) the Mount Gabi seamount and nearby slope-shelf margin at the interface of the Southern and Indian oceans; with new information from (3) the Perth Canyon Marine Park located in the SE Indian Ocean. These canyons differ from many explored around the world in having no connectivity to continental river systems, thus little detrital input, with the Bremer systems and Mount Gabi facing the Southern Ocean which plays a key role in the global ocean circulation and climate systems. Such studies in the vast deep waters around the Australian continent are rare given the lack of local ROV capability available for research, thus little is known about these environments.

Using the resources of the Schmidt Ocean Institute, we characterised the submarine topography from high-resolution bathymetric mapping, geology, physical and chemical oceanography, and provide an overview of these environments including the fauna observed and collected. We show that these Southern Ocean-influenced environments incorporate South Indian Central Water, Subantarctic Mode Water, Antarctic Intermediate Water, and Upper and Lower Circumpolar Deep Water, with Antarctic Bottom Water present in deep water just south of the Bremer canyon systems. The richness in megabenthos, especially along the steep, rocky substrates of the canyon heads and walls around the Bremer canyon systems, contrasts to the comparatively depauperate fauna of the more northerly Perth Canyon. Various corals serve as important substrates for a range of other species and often exhibit particular faunal associations. Especially notable are distinct ecological zones including a bryozoan and sponge-dominated (animal) forest on the shelf edge, spectacular coral gardens along canyon margins, and the occurrence of solitary scleractinians well below the aragonite saturation horizon. Subfossil coral deposits were discovered across all three study areas, reflecting periodic waxing and waning of deep-water Scleractinia throughout this southwest region. Extensive pre-modern assemblages at Mount Gabi contrast markedly with the sparse populations of living species and suggest that it might have once been a major coral hotspot, or whether they reflect long-term coral aggregations is yet to be determined. Nevertheless, stark differences in both living and past coral distribution patterns across our study sites point to at least localised fluctuations in Southern Ocean-derived nutrient and/or oxygen supplies to these deep-sea communities.

* Corresponding author.
E-mail address: julie.trotter@uwa.edu.au (J.A. Trotter).

https://doi.org/10.1016/j.pocean.2022.102904
Received 24 December 2021; Received in revised form 6 July 2022; Accepted 27 September 2022
Available online 13 October 2022

1. Introduction

A series of Southern Ocean-facing submarine canyons are located along the edge of the continental shelf of southwestern Australia. These ancient canyons extend from the continental shelf-margin to abyssal depths, have no direct landward connection, and probably formed during the Mesozoic rifting of southern Australia from the Indo-Antarctic (Heap et al., 2008, Heap and Harris, 2008, Huang et al., 2014). The canyons around the Bremer Marine Park are famous for attracting the largest seasonal populations of killer whales in the Southern Hemisphere, as well as associated migratory marine life including sperm whales, the southern right whale, dolphins, and sharks. Given that the waters around the southwest Australian coast are largely oligotrophic, canyon topography together with Southern Ocean influences are presumed to play a key role in the supply and upwelling of nutrients, thereby forming hotspots of productivity that likely account for the seasonal populations of cetaceans that transit the Bremer and adjacent canyon systems (Bouchet et al., 2018, Salgado Kent et al., 2020), and the Perth Canyon further north (Rennie et al. 2009a).

Although the abundance of these charismatic fauna has attracted major tourism to this region, the deep-sea habitats of these canyons remain essentially unexplored and largely unknown. Recently, the first remotely operated vehicle (ROV) exploration of the Perth Canyon Marine Park, located in the southeast Indian Ocean, revealed that despite nutrient upwelling and significant marine life activity, the deep-sea megabenthos was surprisingly sparse (McCulloch et al., 2016; Trotter et al., 2018, 2019). An important discovery during that cruise was extensive fossil coral deposits of Last Glacial Maximum age (Trotter et al., 2019; Trotter et al., 2022), increasingly recognised as a major period of climate change important to our understanding of long-term ocean-climate dynamics.

Here we describe our findings from the first ROV expedition to the Southern Ocean-facing canyons (Trotter et al., 2021) in the Bremer Marine Park (Bremer canyon systems) east of Albany, the Mount Gabi seamount and adjacent shelf near the Leeuwin Canyon at the extreme southwestern edge of the Australian shelf, as well as new observations from the Perth Canyon Marine Park (Fig. 1). We had as our prime mission the discovery of still virtually unknown living communities of deep-sea megabenthos and fossil deposits, with a particular focus on corals, and to document their relationship to the highly dynamic Southern Ocean influenced canyon environments. Although many submarine canyons around the world are known for supporting diverse, deep-sea fauna (e.g. Morris et al., 2013; Brooke and Ross, 2014; Quattrini et al 2015; van den Beld et al., 2017; Robert et al., 2020), a key question is whether the proximity of the Bremer systems to the Southern Ocean would offer similar or even enhanced environmental conditions for the growth of deep-water corals that typically support many other benthic and demersal species. Our study also has global significance since the southwest Australian canyon environments are expected to receive nutrients directly from the northern limb of the Southern Ocean overturning circulation system, the main conduit by which nutrients are exported to the thermocline of the world's oceans (Sarmiento et al., 2004). Similarly, understanding the conditions that may have led to the cessation of Southern Ocean nutrient export and resultant widespread regional-scale death beds of fossil deep-sea coral deposits is now highly relevant (Laufkötter et al., 2016; Laufkötter and Gruber, 2018).

This multi-disciplinary study of these deep-sea canyon environments and shallower shelf-margin habitats include analysis of the bathymetry, geomorphology, physical and chemical oceanography, and a preliminary faunal assessment of resident mega- and macrobenthos (also see cruise report, Trotter et al., 2021). In-situ sampling of fauna by ROV specifically targeted live and fossil corals (with associated fauna) throughout different water depths given their potential as environmental archives. Importantly, we also analysed seawater profiles to constrain ambient physical and chemical conditions around these canyon systems. Collectively, these data contribute new, multi-disciplinary information from these unique, rarely studied, deep-water environments, which significantly adds to the few biological surveys of deep-sea habitats further east around the Great Australian Bight (Currie and Sorokin, 2014; Conlan et al., 2015; MacIntosh et al., 2018; O'Hara et al., 2020), and the one previous ROV study of the Perth Canyon (McCulloch et al., 2016; Trotter et al., 2018, 2019).

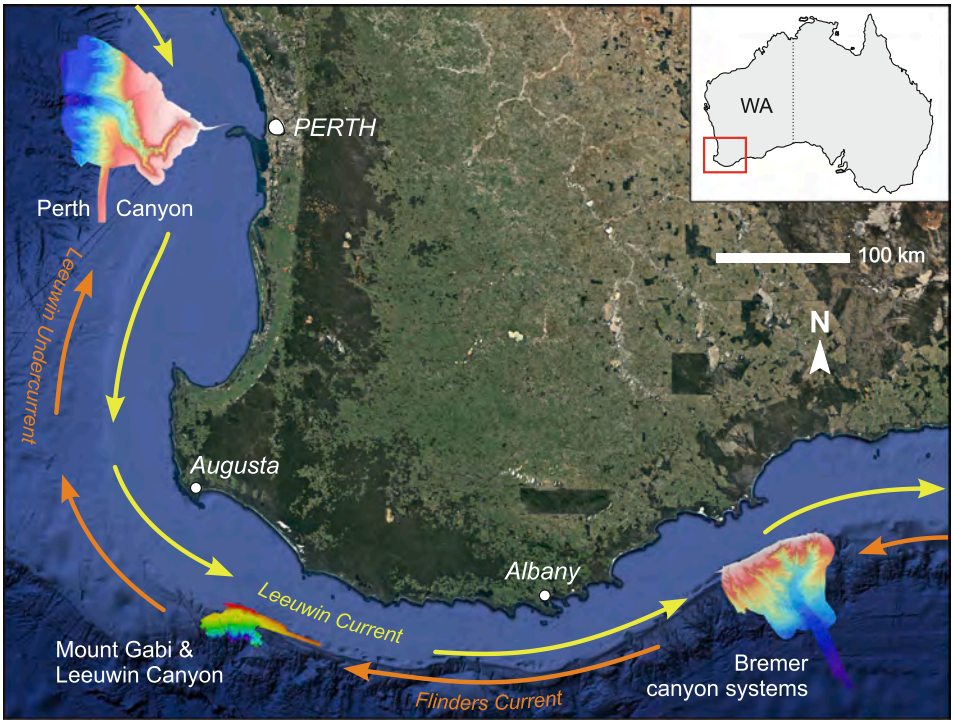

Fig. 1. Location of the three study areas overlain by bathymetry maps generated during the R/V *Falkor* cruise FK200126. The main current systems, Leeuwin Current and Flinders Current, are also shown.

2. Geological setting

The structural architectures along the S-SW passive continental margin of Australia (Supplementary Figure 1) were forged by the evolution of rift margins during the breakup of Gondwana. Along the western margin of southwest Australia, rifting initiated in the Early Permian with ENE-oriented intra-cratonic extension, producing half-graben basins followed by a broad thermal sag basin during the Late Permian to Middle Jurassic (Norvick, 2004). This evolved into a regional NW-SE rifting event from the Late Jurassic, with the complete separation of Australia and Greater India in the Early Cretaceous (Gibbons et al., 2012; Rollet et al., 2013; Hall et al., 2013), producing the NW-SE trending Wallaby-Zenith, the Naturaliste, and Leeuwin Fracture Zones, followed by passive margin subsidence on the shelf edge. Onshore and offshore sedimentary sequences occupy the north–south trending Perth Basin, which extends for about 1300 km along the southwestern continental margin of Australia, its structural configuration on the eastern margin being constrained by the pre-existing Darling Fault System.

Along the southern margin of Australia, the first episodes of rifting commenced slightly later, dating from the Middle-Late Jurassic to Early Cretaceous. The breakup of Australia and Antarctica followed, with seafloor spreading in the Early Cretaceous that initiated from the western and central areas and proceeded towards the eastern part of the southern margin, with separation of the two continents completed in the Tasmania-Cape Adare sector during the Late Eocene (Whittaker et al., 2013; Williams et al., 2019). Such extensional tectonics produced a series of Mesozoic and Cenozoic basins and sub-basins extending for about 2100 km, the geometries, tectonic evolution, and depositional history of which have been recognised from combined onshore geology, limited offshore borehole drilling, seismic reflection data, and dredge results. The Mesozoic sequences in the distal Bight Basin are unconformably overlain by mostly Cenozoic sequences of the Eucla Basin, formed from a more proximal depocentre.

The western part of the Bight Basin occupies a key position, being affected by both the rifting events involving the western and the southern margins of Australia, which formed the Bremer, Denmark, and Recherche sub-basins. The development of these sub-basins was strongly influenced by pre-existing weaknesses along northeast-southwest trending shear zones, which characterise the underlying Proterozoic Albany-Fraser Orogeny and influence the architecture of the deep submarine canyons. Correlation of the dredge samples and shallow gravity cores with seismic data and stratigraphy, as intersected by the Jerboa-1 well 1000 km to the east in the Eyre sub-basin, suggests that initial stages of rifting produced only minor NNW-SSE crustal extension. The sedimentary records in the Bremer and Bight basins mainly comprise syn-rift fluvial sandstone and lacustrine mudstone and siltstone of Jurassic age (Totterdell et al., 2000; Blevin and Cathro, 2008), which are overlain by Early Cretaceous (Berriasian to Albian) fluvio-lacustrine to marine sediments with onlapping geometries suggesting deposition during a period of thermal subsidence. During the Late Cretaceous, a pronounced transgression is documented by the deposition of marine shales, which marks a clear acceleration of crustal extension (Totterdell and Bradshaw, 2004). These sequences are unconformably overlain by the Cenozoic sediments of the Eucla Basin (Bradshaw et al., 2003), formed during the final stages of separation between Australia and Antarctica (Totterdell et al., 2000). Offshore, Miocene to Pleistocene deep-sea chalks and oozes represent the syn- and post-rifting open marine phases (Bradshaw et al., 2003).

3. Oceanographic setting

Two major boundary currents flow along the southern region of Western Australia (Wijeratne et al., 2018; Akhir et al., 2020; Fig. 1): (1) the eastward flowing Leeuwin Current (LC) along the shelf break (to ~300 m depth); and (2) the westward flowing Flinders Current (FC), with its core located further offshore close to the continental slope at ~400–500 m depth (Duran et al., 2020). The FC flows as an undercurrent beneath the LC and further offshore as a surface current (Wijeratne et al., 2018; Akhir et al., 2020). The LC originates from the North-West Shelf region of Australia, flows poleward to Cape Leeuwin, then turns east into the Great Australian Bight and across to the southern tip of Tasmania, thereby forming the longest (~5500 km) boundary current in the world (Ridgway and Condie, 2004). In summer it transports warmer and relatively higher saline South Indian Central Water (SICW) southward and eastward to depths of ~250 m (Cresswell and Peterson, 1993). The LC, however, does not directly interact with the submarine canyons that are in water depths >500 m (Rennie et al., 2009b). The FC forms off the coast of Tasmania and flows westward to Cape Leeuwin to a maximum depth of 800–1000 m (Middleton and Bye, 2007; Duran et al. 2020), then northwards where it is known as the Leeuwin Undercurrent.

The FC transports the Subantarctic Mode Water (SAMW), which contains higher dissolved oxygen concentrations, that is formed through deep winter convection at 40-50°S in the region south of Australia, between the subtropical convergence and the subantarctic front (McCartney, 1977; Wong, 2005, Woo and Pattiaratchi, 2008). South of Australia, the SAMW is found at depths between ~300 and ~750 m associated with the FC. The high dissolved oxygen (DO) reflects the relatively young age of this water mass that is formed every winter. Upwelling onto the continental shelf seems to be controlled by the interaction between the westward flowing FC and the submarine canyons (Kämpf, 2007, 2021). Underlying the SAMW is the Antarctic Intermediate Water (AAIW), an intermediate layer between ~800 and ~1300 m water depth (Woo et al., 2006) and characterised by a salinity minimum, which is formed in the Antarctic Polar Zone (Molinelli, 1981; Fine, 1993; Sloyan and Rintoul, 2001). AAIW overlies the Upper Circumpolar Deep Water (UCDW), which occurs at depths of ~1500 to ~2600 m and has a DO minimum (Woo et al., 2006). The underlying Lower Circumpolar Deep Water (LCDW) is present within a depth range of 2600–3500 m and is characterised by a salinity maximum and higher DO concentrations. The Antarctic Bottom Water (AABW) lies beneath the LCDW and flows northward into the South Australian Basin at depths below ~4100 m (Woo et al., 2006). AABW is the densest water mass found in the world's oceans (Tomczak and Liefrink, 2005) and has relatively high DO concentrations, indicating a younger and more ventilated water mass than LCDW and UCDW. See Results (Figs. 6-8) for seawater profiles and water mass depths in the BCS and PC.

4. Materials and methods

Cruise FK200126 was undertaken during the austral summer from January 26th to February 26th 2020 aboard R/V *Falkor*, the research vessel of the Schmidt Ocean Institute non-profit foundation. *Falkor*'s multibeam sonar systems (Kongsberg EM 302 and 710) were used to generate high-resolution bathymetric and geomorphic maps, which encompassed an area >11,000 km^2. These maps were the basis for identifying prospective deep-water coral sites (see 4.3) within our three study locations:

1. The Bremer canyon systems: Southern Ocean ~175 km E of Albany, around the Bremer, Hood, Henry, and Knob canyons (Fig. 2);
2. North of the Leeuwin Canyon: Southern Ocean ~90 km SSE of Augusta, around Mount Gabi, and ~6 km north on the continental slope and scarp (Fig. 3);
3. The Perth Canyon: southwest Indian Ocean, ~60 km W of Perth (Fig. 4).

The Schmidt Ocean Institute's remotely operated vehicle (ROV) *SuBastian*, surveyed the deep-sea habitats and collected data and samples during 17 dives (Figs. 2-4). *Falkor's* CTD-Rosette system was used to measure seawater parameters in-situ and characterise the major water masses, however technical difficulties and/or poor weather conditions limited its deployment to 18 sites within the Bremer and Perth canyon

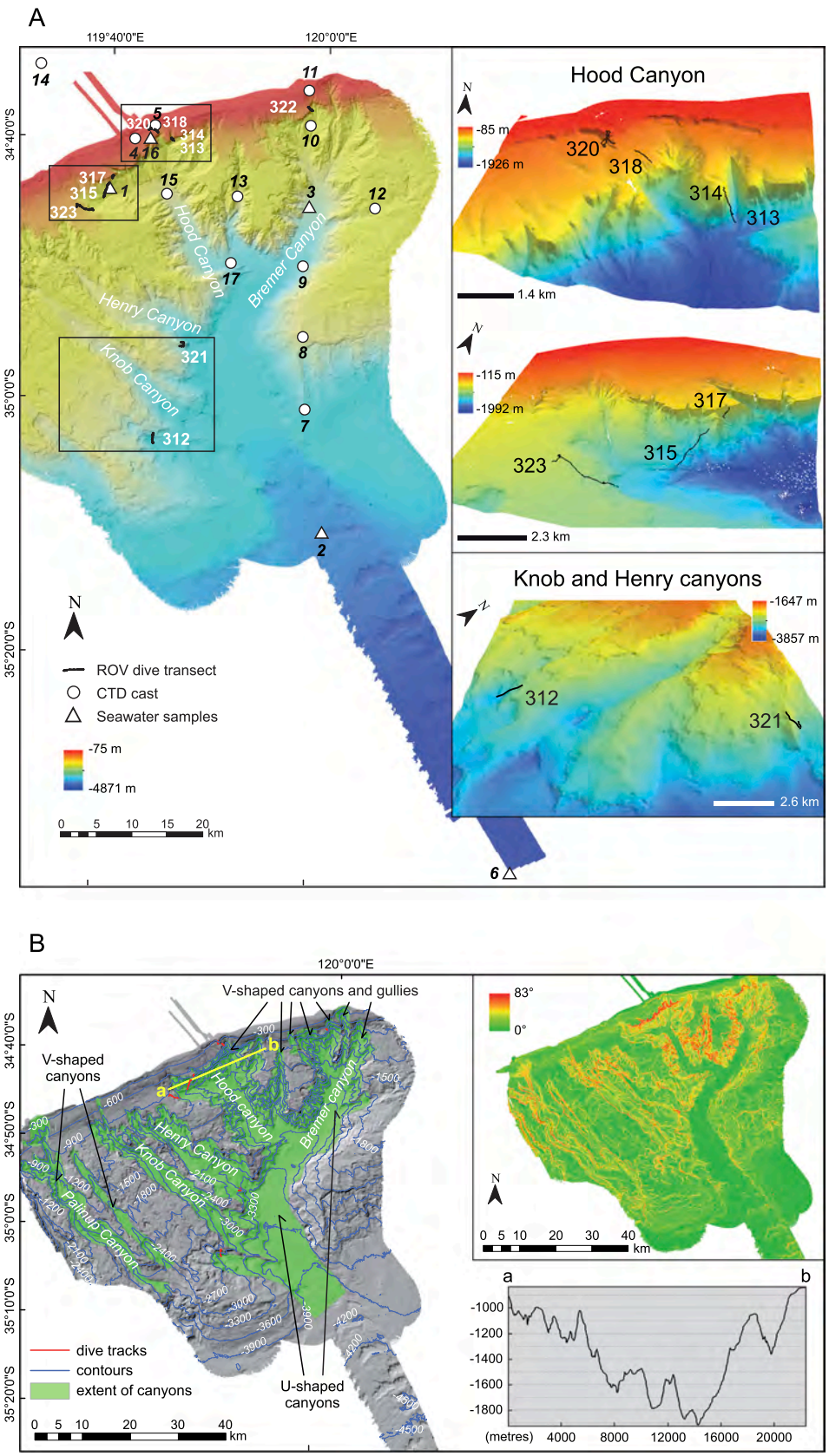

Fig. 2. (A) Bathymetric map of the Bremer canyon systems (30 m resolution, 2x vertical exaggeration) showing CTD-Rosette cast and ROV dive sites. Insets show 3D view of the MB Bathymetry (20 m resolution, 2x vertical exaggeration) near dive transects at the head of the Hood Canyon (top right), its western limb (centre right), and proximal to the Henry and Knob canyons (bottom right). (B). Hillshade (illumination angle 315°, 2x vertical exaggeration) and contour map (300 m intervals) of the Bremer canyon systems. Green shading represents the extension of the canyons. Yellow line (a-b) defines path of cross section showing the complex morphology of the head of the Hood Canyon (bottom inset). Slope map is derived from the MB bathymetry calculated in degree (top inset). Bathymetry and hillshade maps show the main canyons comprising this system, the Bremer Canyon, Hood Canyon, Henry Canyon, and Knob Canyon, which relate to the ROV dive sites.

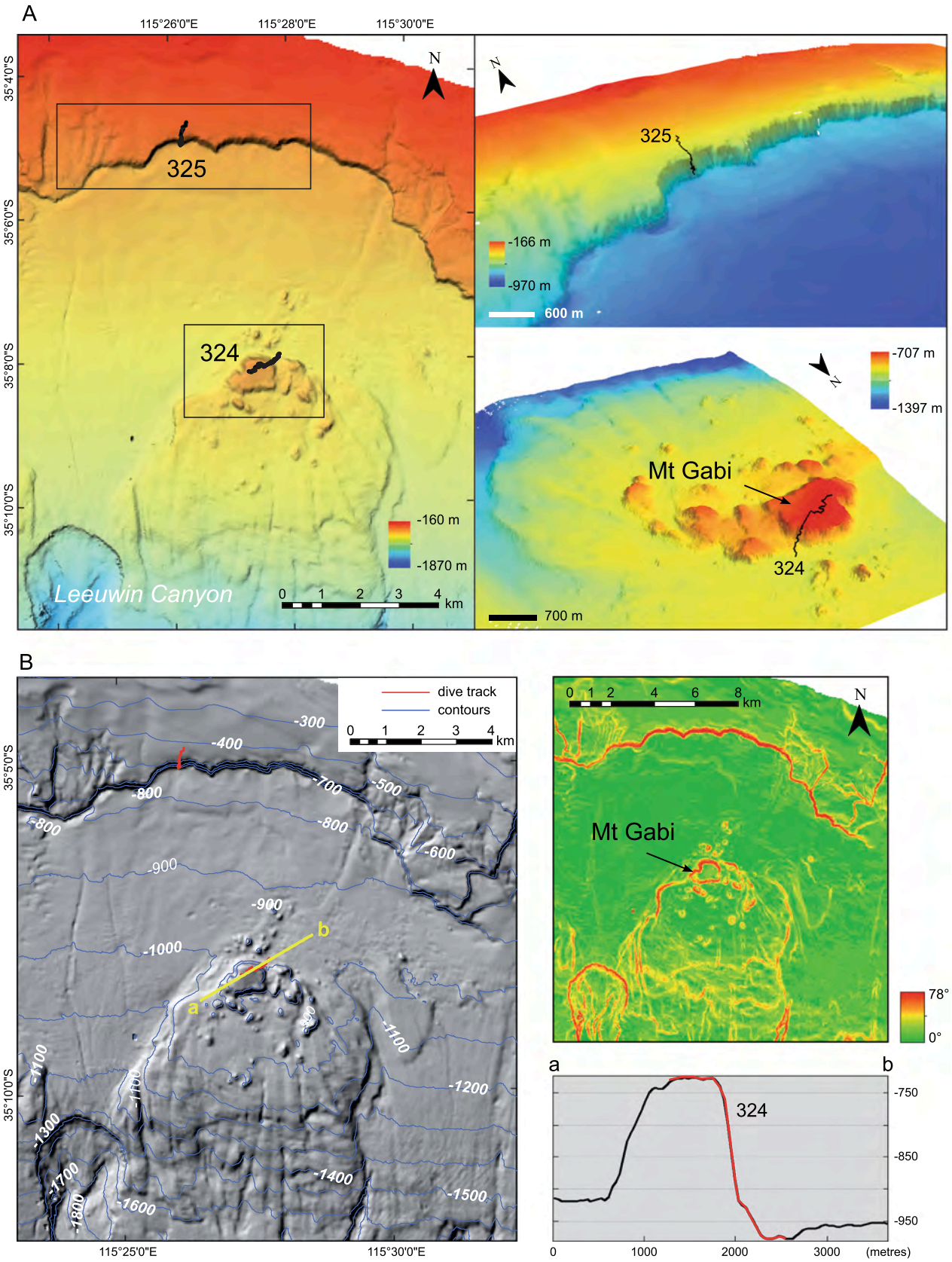

Fig. 3. (A) Bathymetric maps and 3D views (40 m resolution, 10x vertical exaggeration) showing dive transects along the continental slope-shelf (top inset) and Mount Gabi (bottom inset), north of the Leeuwin Canyon. (B). Hillshade (illumination angle 315°, 10x vertical exaggeration) and contour (100 m intervals) map of continental slope-shelf and around Mount Gabi. Yellow line (a-b) defines path of cross section of Mount Gabi (bottom inset). Slope map is derived from the MB bathymetry calculated in degree (top inset).

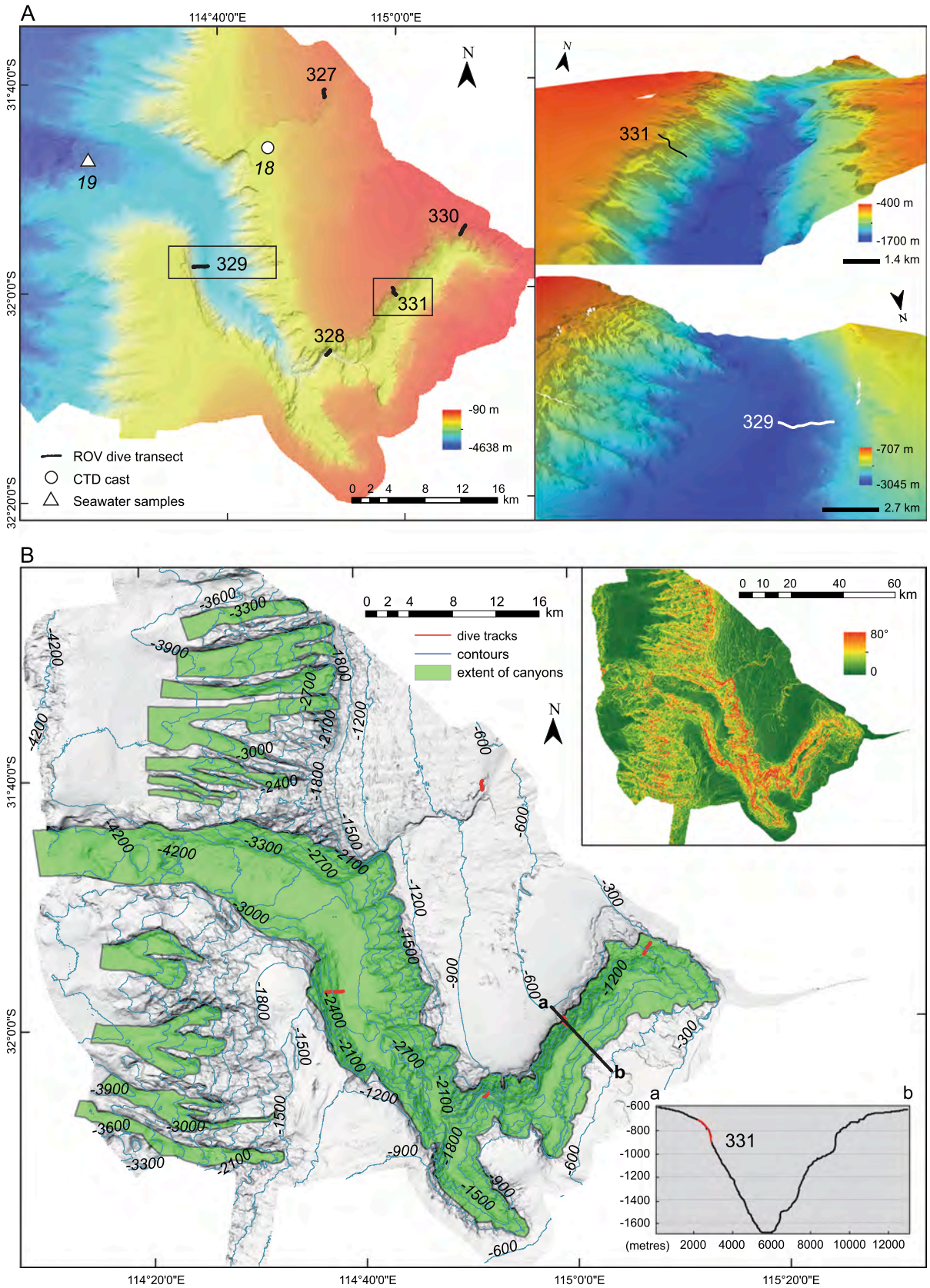

Fig. 4. Bathymetric map of the Perth Canyon (40 m resolution, vertical exaggeration 10x) showing CTD-Rosette cast and ROV dive transect sites. Insets show 3D view of the MB bathymetry (30 m resolution, vertical exaggeration 10x) near dive transects 331 in the NE-SW tributary (top inset) and 329 in the NW-SW limb near the mouth of the canyon (bottom inset). (B). Hillshade (illumination angle 315°, 10x vertical exaggeration) and contour (300 m intervals) map of the Perth Canyon. Green shading represents the extension of the Perth Canyon and black line (a-b) defines path of cross-section of the NE-SW tributary near dive 331 (bottom inset). Slope map is derived from the MB bathymetry calculated in degree (top inset).

systems (Figs. 2, 4). See FK200126 cruise report for further details (Trotter et al., 2021).

4.1. Multibeam bathymetric analysis

High-resolution bathymetric data were acquired using Kongsberg EM 302 and 710 multibeam echo sounders, and processed both onboard and post-cruise, with bathymetry maps of the canyons and all dive sites generated at different spatial resolutions. The multibeam echo-sounder data was processed onboard using Qimera software. After loading raw data and applying tide corrections, a dynamic surface at variable resolution (from 10 to 30 m) was created using the cube options. The data were 'cleaned' using the Swath Editor that consists of interactively selecting and rejecting soundings as well as filtering functions, which automatically detected and rejected outliers. Following data correction and cleaning, a digital terrain model (DTM) was generated at 30 m resolution for each canyon, and at higher resolution (from 10 to 20 m, depending on the water depth) for the ROV dive areas (Figs. 2-4). The DTMs were exported in ASCII ESRI format and analysed with ArcGIS 10.5. The ArcGIS Spatial Analyst tool was applied to derive the hill shade from the DTM with a vertical exaggeration of 1.5.

4.2. Seawater collection and analyses

The physico-chemical parameters of the major water masses were analysed in-situ at 16 locations around the Bremer canyon systems, and 2 sites at the Perth Canyon (Figs. 2, 4). At six of those sites, depth profiles of seawater samples (n = 101) were collected for detailed hydrochemical and stable isotope analyses (Supplementary Table 1, Supplementary Figures 2–7), five casts in and around the Bremer canyon systems (n = 82) and one cast (n = 19) near the mouth of the Perth Canyon. Water samples were collected between 5 and 4810 m from 12 L Niskin bottles mounted on a Rosette system equipped with a Seabird SBE 911plus CTD, with a SBE 43 dissolved oxygen sensor and Wet Labs ECO-FLNTU fluorescence sensor. Water column profiles were based on measurements of pressure (depth), temperature (T), conductivity (salinity: S), dissolved oxygen (DO), total alkalinity (TA), dissolved inorganic carbon (DIC), dissolved inorganic nutrients, and stable isotopes (δ^{13}C of DIC, δ^{2}H and δ^{18}O of H_2O), together with calculations to determine the full suite of carbonate chemistry parameters (see below).

Seawater dissolved inorganic carbon (DIC) was measured on board using an Apollo SciTech Dissolved Inorganic Carbon analyser following the SOP2 of Dickson et al. (2007). Seawater TA was measured on board and post-cruise at The University of Western Australia, using a Mettler-Toledo T50 with Rondolino autosampler following the open-cell titration approach described in SOP3b from Dickson et al. (2007), and 'Seacarb' R-code for TA calculations (Comeau et al., 2017). For both DIC and TA measurements, CRM reference (Batch-187) material prepared at the Scripps Institution of Oceanography of the University of California, San Diego, was used (Dickson et al., 2003). Internal errors for DIC and TA based on CRM measurements were 0.2 % and 0.08 % (1σ RSD) respectively. The external error for TA measurements were calculated by repetitive analyses (every eighth sample) of seawater samples collected at the beginning of the cruise (surface water), which measured 2381 ± 1.7 (0.07 %, 1σ RSD). The external error for TA samples from cast 02C were higher (0.52 %, 1σ RSD) due to issues with the titrator.

Seawater pH (total scale), pCO_2, calcite saturation state ($\Omega_{calcite}$), and aragonite saturation state ($\Omega_{aragonite}$) were calculated post-cruise using version 1.1 of CO2SYS for MATLAB (van Heuven et al., 2011), based on the dissociation constants for carbonic acid from Lueker et al. (2000), sulfate from Dickson (1990), and borate from Lee et al. (2010).

Dissolved inorganic nutrients, including ammonium ($N\text{-}NH_4^+$), nitrate + nitrite ($N\text{-}NO_x^-$), phosphate ($P\text{-}PO_4^{2-}$), and silicate ($Si\text{-}SiO_3^{2-}$) were analysed at The University of Western Australia on a Lachat autoanalyser (QuickChem QC8500) and a fluorescence detector (Waters 747) for NH_4^+.

Seawater barium (Ba) concentrations were undertaken using standard isotope dilution protocols, the seawater unknowns diluted x100 with 2 % HNO_3 and spiked with ^{137}Ba, then analysed using a high sensitivity Thermo Scientific Element 2. The isotopes of Ba (130, 132, 134, 136, 135, 137, 138) were measured together with cerium (^{140}Ce) and xenon (^{131}Xe), the latter for interference corrections. The seawater unknowns were bracketed by an in-house seawater standard and cross-checked with analyses of NIST3104a and certified seawater standards. Ba concentrations are reported in nmol/kg with an analytical uncertainty of 0.9 % (2σ RSD).

Stable carbon isotope analyses of dissolved inorganic carbon ($\delta^{13}C_{DIC}$) were undertaken in the West Australian Biogeochemistry Centre at The University of Western Australia. Seawater $\delta^{13}C_{DIC}$ compositions were analysed using a Thermo Fisher GasBench II coupled with Delta XL Isotope Ratio Mass Spectrometer. DIC was reacted with 0.1 mL of 100 % H_3PO_4 at 25 °C for 24 h (Paul and Skrzypek, 2006). All results were expressed using the standard delta-notation (δ^{13}C) and were reported in permille (‰) after normalization to Vienna Pee Dee Belemnite isotope scale [VPDB]. Normalization was based on two international standards NBS18 (-5.01 ‰), NBS19 (+1.95 ‰), and verified using L-SVEC and laboratory standards (Skrzypek, 2013). The analytical uncertainty was ≤ 0.1 ‰ (1σ SD).

Stable hydrogen and oxygen isotope compositions of seawater samples were analysed using a Picarro 2130 Isotopic Liquid Water Analyser in the West Australian Biogeochemistry Centre at The University of Western Australia (Skrzypek and Ford, 2014). The δ^{2}H and δ^{18}O raw values were normalized to the VSMOW (Vienna Standard Mean Ocean Water) scale following the principles of the three-point normalization (Skrzypek, 2013). Three laboratory standards were calibrated against international reference materials that determine the VSMOW-SLAP scale (Coplen, 1996), provided by the International Atomic Energy Agency (for VSMOW2 δ^{2}H and δ^{18}O = 0 ‰, and for SLAP2 δ^{2}H = -428.0 ‰ and δ^{18}O = -55.5 ‰). The long-term analytical uncertainty was determined as < 1.0 ‰ for δ^{2}H and < 0.1 ‰ for δ^{18}O (1σ SD).

Seawater profiles of CTD-Rosette data were prepared using Ocean Data View software (version 5.3.0; Schlitzer, 2020).

4.3. Faunal and geological sampling

The ROV *SuBastian* surveyed the deep-sea environments and habitats using HD and 4 K UHD cameras, which generated approximately 160 h of video footage, and collected representative samples of megabenthos, sediments (push cores and scoops), and rocks (Trotter et al., 2021). Seawater parameters (T, S, DO) were also measured in-situ using the onboard CTD sensors.

The dives were undertaken at 17 sites (Table 1; Figs. 2-4), mostly selected on the basis of anticipated hardgrounds and steep topographies inferred from backscattered bathymetric mapping. Although a wide range of depths were surveyed, intermediate and mode water intervals along the rocky canyon walls were a primary focus, potentially being the most prospective for coral sampling. The ROV descended rapidly to commence transects after reaching the substrate at the pre-determined depth then meandered forward gradually ascending searching for suitable habitats. Logging of observations and sampling events using Squidle+ and Sealog software usually commenced at bottom-depth, mostly based on forward looking vision (although rear cameras were monitored). High resolution video footage was taken throughout each dive from launch till retrieving the ROV, with framegrabs taken automatically at 5-second intervals as well as manually on occasion including during sample collections. Transect paths were not predetermined, nor was a systematic gridded transect and sampling approach taken, given that the primary objective was to locate and sample corals for post-cruise geochemical analysis rather than undertake comprehensive ecological surveys. The dives were typically

Table 1
Dive information for each study area. Approximate depth range of benthos observed and dominant substrate traversed. BCS = Bremer canyon systems. SICW: South Indian Central Water; SAMW: Subantarctic Mode Water; AAIW: Antarctic Intermediate Water; UCDW: Upper Circumpolar Deep Water; LCDW: Lower Circumpolar Deep Water.

Location	Depth (m)	Dive	Water Mass	Substrate / Comments
Hood Canyon (BCS)	180–390	320	SICW-SAMW	muddy and rubble shelf flats
Hood Canyon (BCS)	430–510	318	SAMW	muddy and rubble shelf flats
Bremer Canyon (BCS)	640–1130	322	SAMW-AAIW	rocky walls, muddy shelf, fossil coral
Hood Canyon (BCS)	650–1380	314	SAMW-UCDW	rocky walls, fossil coral
Hood Canyon (BCS)	715–1090	317	SAMW-AAIW	rocky walls, muddy flanks
Hood Canyon (BCS)	910–1280	323	AAIW-UCDW	rocky walls, muddy flanks
Hood Canyon (BCS)	1160–1550	315	AAIW-UCDW	muddy floor, rocky flanks
Hood Canyon (BCS)	1220–1540	313	AAIW-UCDW	muddy flanks, rocky walls
Henry Canyon (BCS)	2560–3020	321	UCDW-LCDW	muddy floor, rocky flanks
Knob Canyon (BCS)	2770–3300	312	UCDW-LCDW	muddy floor, rocky flanks
Leeuwin shelf-slope	430–760	325	SAMW-AAIW	rocky walls, muddy shelf flats
Mount Gabi	720–970	324	SAMW-AAIW	rocky walls, extensive fossil coral
Perth Canyon	390–710	330	SAMW	rocky walls, muddy shelf flats
Perth Canyon	670–740	327	SAMW	rubble terraces, extensive fossil coral
Perth Canyon	770–1120	331	AAIW	rocky walls, muddy flank
Perth Canyon	1800–2260	328	UCDW-LCDW	muddy floor, rocky walls
Perth Canyon	2530–3000	329	LCDW	muddy floor, rocky flanks

undertaken each day within approximately 8 to 10 h intervals during daylight hours.

Collectively, the dives spanned depths from ~180 to ~3300 m, with deep-water corals (predominantly calcifiers) collected between 334 and 2896 m. All faunal sampling was strictly limited by quotas under the Federal (Commonwealth Marine Park) and Western Australia State permits. Survey descriptions reported here are mostly based on real-time observations of video footage recorded in the event logs, but also supplemented by some post-cruise assessments of samples, videos, and framegrabs. Given that real-time log entries were often undertaken by non-specialists, identifications thus-far are given at high taxonomic levels or genus where possible (Supplementary Table 2). Accordingly, more robust determinations and quantitative assessments are dependent on future analysis by various specialist workers of the video footage and specimens collected.

The bulk of live-caught and dead coral samples are in the Chief Scientist's (J. Trotter) collection at The University of Western Australia, with vouchers of collected specimens deposited with the Western Australian Museum, Perth. Also see Trotter et al. (2021) for further details.

4.4. Coral distribution assessment and statistical analyses

Real-time biological observations logged during each dive were used to compare taxonomic richness and coral abundances, which were also differentiated by skeletal composition (aragonite, calcite, proteinaceous), substrate type (hard, soft), dive site, and study area.

Species accumulation curves (SAC), describing the number of species or distinct classes observed per new frame (sample) analysed (*sensu* Cordes et al., 2010), were generated using function "specaccum" of package "vegan" (method "random", 1000 permutations, version 2.5–7). The number of frames needed to document 70 % of the observed taxa was used to randomly sub-sample framegrabs, generating 3 sub-transects per dive video. Taxa abundances were calculated by counting the number of observations in every sub-transect. Information on the different compositions of cnidarian skeletons was also reported to explore the distribution of aragonitic, calcitic, and proteinaceous taxa in the surveyed sites.

The significant difference in the composition of macro and megabenthic epifauna among the three surveyed areas was tested using ANOSIM (analysis of similarities) in R software (package: vegan, version 2.5–7). The normal distribution and homogeneity of variance of taxonomic richness and hard cnidarian abundance amongst the explored canyons were checked using the Shapiro-Wilk test (package "stats", version 4.2.0) and Levene's test (package "car", version 3.0), respectively. Since the assumptions were not fulfilled, differences were tested using Kruskal–Wallis test and non-parametric pairwise comparisons Dunn's test in R software (R Core Team, 2019).

5. Results

5.1. Geomorphology of the canyon systems

5.1.1. Bremer canyon systems

The portion of the Bremer Sub-Basin surveyed (Trotter et al., 2021) encompasses an array of seven submarine canyons deeply incised from the uppermost slope down to the base of the scarp, extending over an area of about 4,380 km^2 and into the Albany canyon group. The Bremer Canyon, Hood Canyon, Henry Canyon, and Knob Canyon are part of the broader Bremer canyon systems, hereafter referred to as the BCS (Fig. 2).

The Bremer Canyon, located on the easternmost side of the study area, has five main V-shaped branches, which almost reach the shelf break at a depth range between 140 and 380 m and merge at about 2200 m into the wide almost flat and U-shaped Bremer channel. The orientation of the canyon branches varies from SW to SE, while the main Bremer channel runs oblique to the continental shelf edge bending mostly SW. The canyon slope angle reaches 60° within the canyon head, with the westernmost flanks becoming steep cliffs. The head of the canyon is breached by multiple gullies up to a depth of 900 m.

The Hood Canyon deeply incises the continental slope with a wide and meandering head of about 40 km long between water depths of 500 to 600 m. The rim of the canyon head is associated with an abrupt increase in seafloor gradient from about 10° to 65°, with the slope of the canyon gradually diminishing seawards. The canyon head is V-shaped with multiple tributaries that connect to a single channel that is about 2500 m deep and about 5 km wide and runs almost perpendicular to the shelf break in a SE orientation. One of the small eastern tributaries runs W-E parallel to the shelf break, which abruptly changes orientation where it meets the other branches.

The Henry and Knob canyons run straight down to the slope to the southeast and merge at about 3400 and 3600 m respectively into the 16 km wide U-shaped channel that connects the four canyons. The canyon

heads incise the slope with a gradient of about 40° from 650 to 900 m. A minor V-shaped tributary of the Knob Canyon almost reaches the shelf break at about 180 m.

Towards the flanks of these canyons the sediments become muddy but with rocks outcropping within gullies or scarps. All canyons have complicated networks of gullies in the upper flanks and numerous headwall scarps with evidence of slump and slope failures, and consequent gravity driven flows causing retrogressive canyon wall failure.

5.1.2. Leeuwin Canyon region

The area mapped around the Leeuwin Canyon (Trotter et al., 2021) encompasses the upper portion of the continental slope reaching the shelf break, Mount Gabi seamount, and an array of five slope-confined blind submarine canyons (Fig. 3).

The upper slope gently deepens southwards (average slope of about 5-6°) and is characterised by the presence of a long scarp (13 km) with steep walls of ~60° degrees that ranges from 500 to 600 m water depth. The upper slope is incised by multiple gullies converging southwards into the main canyon system and is generally dissected by several smaller scarps with walls of about 20°.

Mount Gabi lies 10 km south of the continental shelf edge, and spans 5 km wide and 300 m high from depths of ~700–1000 m. The gradient of the north flank is ~60° while the south side has a gentler slope of up to ~40°. This seamount is surrounded by several smaller relief structures, being a maximum of 120 m high, 300 m wide, with slopes reaching 50°.

The blind Leeuwin Canyon system comprises multiple heads that are located at depths between 950 and 1300 m and are generally U-shaped. The rims of the canyon heads have steep walls from 20 to 40°. The canyon axes are simple in form and run straight down to the slope.

5.1.3. Perth Canyon

The Perth Canyon (hereafter referred to as PC) is the second largest submarine canyon on the Australian continental margin and the largest in waters off the southwest coast; it covers an area of >1500 km^2 and has a depth range of >4000 m (Fig. 4). This long (125 km) canyon has two well-defined tributaries that form a sinuous V-shaped configuration, extending across the slope to the abyssal plain. The head of the canyon partly incises the continental shelf, being unconnected from the coast and adjacent Swan River.

The surveyed area (Trotter et al., 2021) included a portion of the continental shelf that is incised by long and steep (~30°) escarpments, oriented E-SW and perpendicular to the shelf edge (i.e. near dive 327). The walls of the canyon typically reach a slope from 30° to 40° although some parts especially in the deepest sector are near vertical (~70°). The canyon has well-defined arcuate headwalls, subparallel sidewalls, and smooth failure surfaces. The direction of landslide movement is predominantly perpendicular or quasi-perpendicular to that of the canyon thalweg. Around the canyon there are numerous smaller blind canyons along the continental slope from 1700 to 3900 m water depth. These canyons run E-W, straight down to the Perth abyssal plain, parallel to the deepest arm of the canyon.

5.1.4. Major geomorphic features

The four major features identified in the Bremer, Hood, and Perth canyons are: (1) vertical walls, (2) gentle slopes, (3) terraces, and (4) flat expanses, and various combinations of these features (Fig. 5A-D, Supplementary Figure 8). The [near] vertical walls commonly form where the bedrock is crystalline or comprised of well-lithified sedimentary rock units. The BCS have cliffs tens of metres high where basement crystalline rocks predominate but also incorporate overlying Mesozoic sedimentary rocks (Supplementary Figure 8A) and Cenozoic chalks (Fig. 5C). The PC comprises the equivalent Mesozoic-Cenozoic sedimentary sequence, although the obvious younger Cenozoic carbonates appear thicker and more widespread. Gentle slopes are diffuse and often blanketed by fine sediments. Outcropping chalk units commonly form mound structures (Fig. 5K) and terraces are most evident on the upper sedimentary units (Fig. 5C). Flat muddy expanses occur along the canyon floors and flanks (Fig. 5D) or shoulders where rocky units are absent, as well as the shallow areas above the canyons.

5.2. Geology

ROV visual records provide the first in-situ information about the geology (Fig. 5, Supplementary Figure 8) of the areas around the BCS and north of the Leeuwin Canyon.

Crystalline basement rocks crop out between 770 and 1520 m in the Hood and Bremer canyons. Such lithologies (Fig. 5E-G) represent the hardest substrate typology identified in the southwestern Australian canyons studied and form dramatic topographies with towering cliffs and rocky falls (Fig. 5F-G). Features, such as fractures and joints, were observed during the ROV surveys (Fig. 5G), and metamorphic rocks (e.g. granitoids, quartzite, micaschist) were observed and collected. The basement rocks lie below siliciclastic sequences, which in the BCS comprise Mesozoic siliciclastic rocks seen at many dive sites (Fig. 5H-I, L). Hand samples are dominated by medium- to coarse-grained quartz-rich feldspar-bearing sandstone, subordinate conglomerate, laminated mica-rich fine-grained sandstone to siltstone, and claystone. These rocks most commonly outcrop between 2310 and 3262 m, and locally at shallower depths (650–700 m) near the heads of the canyons. Mesozoic?-Cenozoic carbonate rocks are also common, generally represented by grainstone and rudstone (Fig. 5J), sometimes highly fossiliferous and encasing molluscs, coral and bryozoan bioclasts (≤1 cm), packstone and wackestone to floatstone with millimetre-sized bioclasts and variable siliciclastic components, and pale-yellow to grey and yellowish-brown mudstone. In general, limestones stratigraphically lie above siliciclastic sequences. Such carbonates outcrop in the Hood Canyon, observed at depths of 305 m, 488 m, and 1520 m, and were collected at 2917 m further offshore near the mouth of the adjacent Henry Canyon. The youngest carbonates are white or pale yellow-grey very fine-grained, weakly consolidated and friable chalks (Fig. 5K), often displaying intense bioturbation.

Putative Mesozoic sandstones also occur at Mount Gabi (910 m), north of the Leeuwin Canyon. Carbonate rocks, predominantly Cenozoic friable chalk, were collected at 965 m. In the PC, sandstones of possible Mesozoic age were observed between 1792 and 2950 m, while Mesozoic-Cenozoic carbonate rocks were collected from outcrops at depths from 668 to 2647 m.

Of the recent sedimentary features, hemi-pelagic mud typically drapes over the canyon slopes (Fig. 5L) and predominantly occurs at bathyal depths and along the canyon floors. Carbonate ooze with resuspended sediments from Cenozoic chalky bedrock is especially obvious in the BCS. The muddy bottom of the canyon floors is intensely bioturbated from infaunal organisms, mobile macrofauna, and demersal species (Fig. 5D). In places, coarse constituents, such as skeletal remains, are concentrated at the foot of some scarps or next to boulders. Coarse shell deposits (Fig. 5O) were also frequently observed on terraces and at the foot of cliffs often next to their producers (e.g. echinoids, bivalves, corals and sponges). Large aprons of gravity-driven deposits comprise slumped blocks, rock falls, and locally confined gravel accumulations (Fig. 5N). Downslope, at the foot of a chalky escarpment in the Hood Canyon (1530 m), gravelly carbonate hash deposits contain biosomes and bioclasts of shallow-water molluscs (*Tricolia, Cardita*) and barnacles mixed with deep-water species. Fields of megaripples were a striking feature along the top of Mount Gabi (Fig. 5M).

5.3. Physical and chemical oceanography

The key physico-chemical parameters of temperature (T), salinity (S), and dissolved oxygen concentration (DO), were measured in-situ to identify the major water masses (Table 2; Figs. 6 and 7; see also Trotter et al., 2021) in real-time, which assisted with dive site selection and

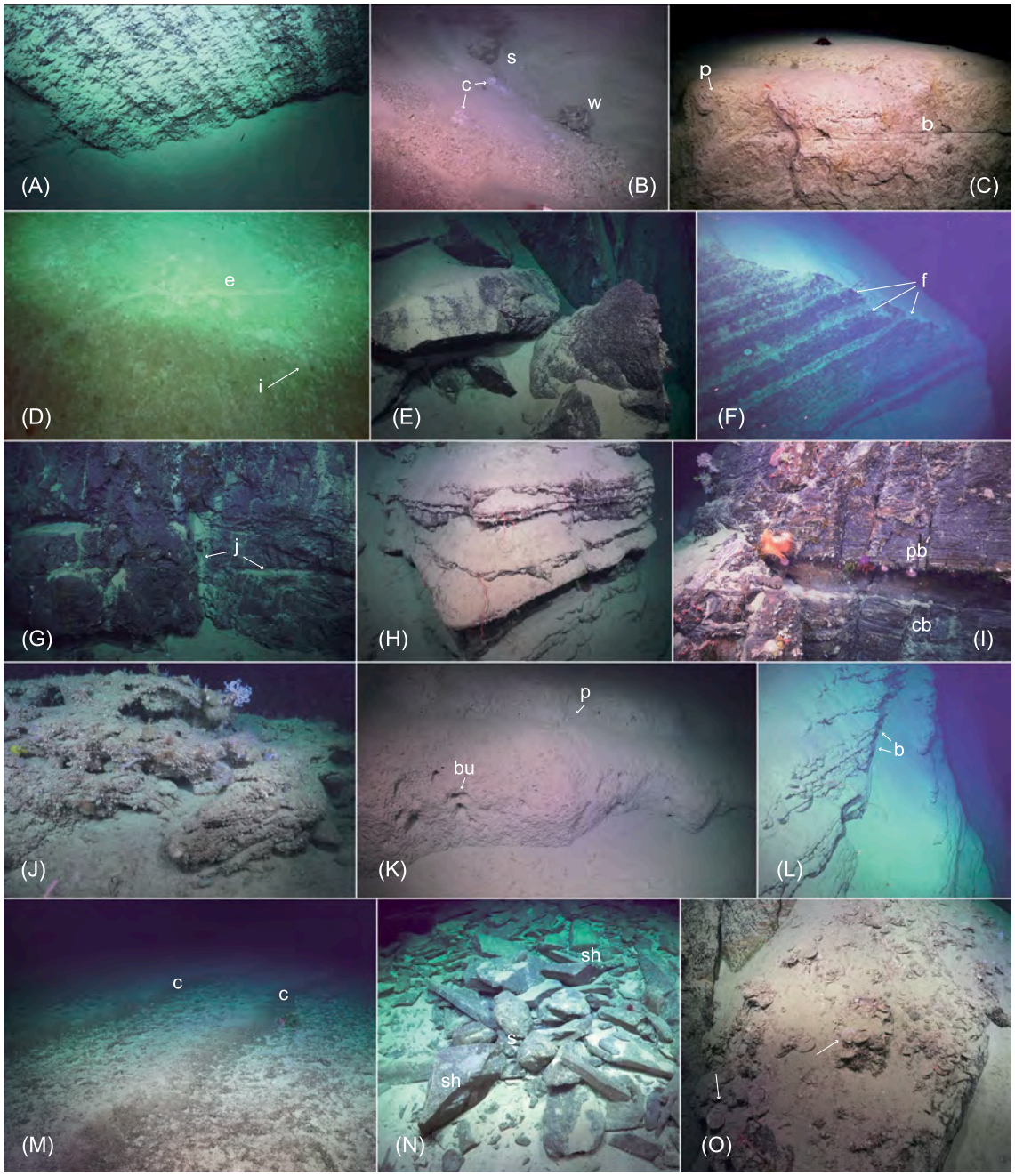

Fig. 5. Representative geological and geomorphological features. (A) Vertical wall comprising layered Mesozoic sandstone–siltstone, Hood Canyon, dive 323, 1209 m; (B) Mass gravity deposit of blocks and gravel comprising chalk (white, c) and sandstone (dark, s) lithologies, as well as whale bones (w), Hood Canyon, dive 315, 1531 m; (C) Terraced morphology in Cenozoic chalk bedrock showing bedding (b) and intense biological traces (pits, p), Knob Canyon, dive 312, 2748 m; (D) Carbonate ooze with intense bioturbation by epifaunal (trail, e) and infaunal (i) benthos on canyon floor, Perth Canyon, dive 329, 2857 m; (E) Bedrock and spalling failure of high-grade metamorphics (likely migmatites) from the crystalline basement, probably belonging to the Proterozoic Albany-Fraser Orogeny, Hood Canyon, dive 314, 1054 m; (F) Steep wall exposing metamorphics from the crystalline basement displaying marked foliation (f), Hood Canyon, dive 315, 1465 m; (G) Crystalline basement characterised by almost horizontal and vertical joints (j), Hood Canyon, dive 317, 717 m; (H) Differential erosion in layered Cenozoic? sandstone and siltstone unit draped with recent carbonate ooze, Hood Canyon, dive 315, 1465 m; (I) Mesozoic? sandstones with parallel (pb) and cross (cb) lamination structures, note exploitation of the hard substrate by various cnidarians, Bremer Canyon, dive 322, 836 m; (J) Cenozoic rudstone, Hood Canyon, dive 320, 385 m; (K) Cenozoic friable chalk with erosional and biological features of burrows (bu) and pits (p), Hood Canyon, dive 315, 1513 m; (L) Steep escarpment exposing Cenozoic? sandstones and siltstones beds with distinct layering (b) draped with carbonate ooze, Hood Canyon, dive 315, 1450 m; (M) Megaripples comprising coarse bioclastics (c), mostly subfossil coral deposits, the distance between two crests being ~7 m, Mount Gabi summit, dive 324, 720 m; (N) Rock fall from a submarine cliff, rocks comprise Mesozoic shales (sh) and sandstones (s), Knob Canyon, dive 312, 3262 m; (O) Carbonate skeletal hash enriched in *Acesta* valves (arrow), Hood Canyon, dive 314, 1158 m.

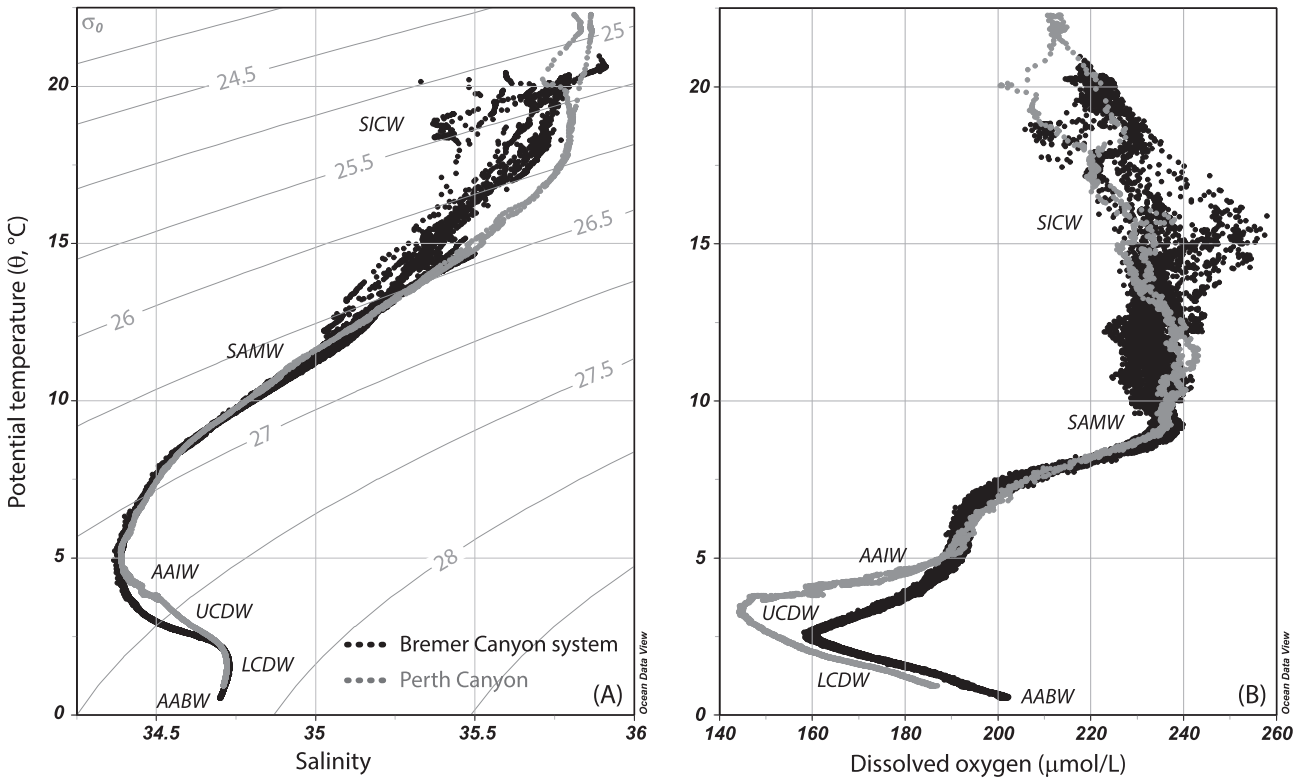

Fig. 6. (A) Salinity versus potential temperature and (B) dissolved oxygen concentrations versus potential temperature from all CTD stations discussed in the paper for the Bremer canyon systems (black) and Perth Canyon (grey).

faunal sampling strategies. Table 1 summarises these properties for the BCS, their minimum and maximum ranges relating to the northward shoaling and variability at shallower depths. Salinity steadily decreased with depth in the BCS, from 35.9 at 30 m (SICW) to a minimum of 34.37 at 970 m (AAIW). Seawater temperature rapidly decreased from ~21–3.4 °C, showing a significant difference between SICW-SAMW and the underlying AAIW. Whilst temperature continued to decrease with depth to a minimum of 0.95 °C at 4800 m (AABW), at the southernmost cast (06C) beyond the mouth of the canyon systems, salinity increased in the transition zone between AAIW and UCDW to a maximum of 34.73 at 2300 m (Fig. 6). The AAIW salinity minimum was centred at ~1000 m and shoaled northward (Fig. 7A), from 1065 m in the open ocean (cast 06C) to 825 m in the northwestern branch of the Hood Canyon (01C). A similar northward shoaling of temperature (Fig. 7B) and DO concentration (Fig. 7C) was recorded, with the depth of the UCDW minimum value shifting from ~1750 m (06C) to ~1550 m (01C). DO concentration was higher and highly variable within the first 500–700 m of the water column, reached a maximum of 255 µmol/L within the SICW-SAMW, decreased to a minimum of 158 µmol/L in the UCDW, and steadily increased to values of ~200 µmol/L at 4800 m in the AABW (Figs. 6B, 7C).

Nutrient concentrations of both N-NO_3 and P-PO_4 increased simultaneously with water depth throughout the BCS (Supplementary Figure 2), resulting in a strong and significant N-P positive correlation (Supplementary Figure 3A, $R^2 = 0.98$, $p < 0.001$) within the upper ~800 m (SICW and SAMW). N-NO_3 increased from ~0 to 34 µmol/kg (0–800 m) and then stabilised at ~41 µmol/kg (36–44 µmol/kg) for depths <800 m. Within this interval, P–PO_4 increased to 1.3 µmol/kg then stabilised deeper at ~2.5 µmol/kg (2.3–2.7 µmol/kg). The most variable concentrations occurred between 700 and 900 m, at the transition zone between SAMW and AAIW. No clear trend was detected in N-NH_4 changes with depth, as these concentrations varied within a large range (0 and 1.10 µmol/kg). Similar patterns were observed for Si-SiO_3 and Ba concentrations (Supplementary Figures 3B, 4, correlation $R^2 = 0.99$, $p <$ 0.001), where constant and low values occurred in the top 300 m of the well-mixed SICW, then progressively increased with depth to ~3800 m (to 138 µmol/kg for Si-SiO_3 and 108 nmol/kg for Ba). Little variation in Si-SiO_3 and Ba concentrations in AABW also shows the high vertical homogeneity of this water mass. The Si-SiO_3 values in SAMW are depleted relative to N-NO_3 (i.e. low silicate-to-nitrate ratio).

Carbonate chemistry (Fig. 8, Supplementary Figure 5) was much more complex given the interactions between pH, salinity, total alkalinity (TA) and dissolved inorganic carbon (DIC). TA in the BCS varied between 2285 µmol/kg at 600 m (SAMW, 03C) and 2408 µmol/kg at 4010 m (AABW, 02C). TA was positively correlated with salinity (Supplementary Figure 5) but the slope and intercept of the regressions are different depending on the depth range, with the shallow-intermediate layers from the surface to ~700–800 m showing a smaller slope (TA/S = 52) compared to the intermediate-deep layers below 800 m (TA/S = 246). DIC steadily increased from the surface (2059 µmol/kg) to ~1500 m (2265 µmol/kg) then stabilised at ~2260 and ~2280 µmol/kg for depths deeper than 1500 m (Fig. 8A, Supplementary Figure 5C). However, the relationship between DIC and TA changed with depth. DIC increased within the upper ~700 m, which was accompanied by a slight decrease in TA (Supplementary Figure 5E). In deeper water masses (AAIW to AABW), the correlation between DIC and TA concentration became positive ($R^2 = 0.72$, $p < 0.001$), and a further increase in DIC (2174 to 2265 µmol/kg at 4810 m) was accompanied by an increase in TA (from 2288 to 2379 µmol/kg at 4810 m), especially between ~800 and 2000 m (Supplementary Figure 5E). At greater depths (>2000 m), TA and DIC show relatively constant values. Calculated pH steadily decreased from 8.19 at 100 m to 7.80 at 4900 m (Fig. 8B). Between 25 and 4800 m, the saturation states for aragonite and calcite decreased from 3.15 to 0.49 and 4.83 to 0.74 respectively, with aragonite undersaturation reached at ~1000 m and calcite undersaturation at 3000 m (Supplementary Figure 6).

The $\delta^{13}C_{DIC}$ values were particularly variable in the top 50 m and ranged from 0.63 to 1.64 ‰ (Supplementary Figure 7A). Below SICW

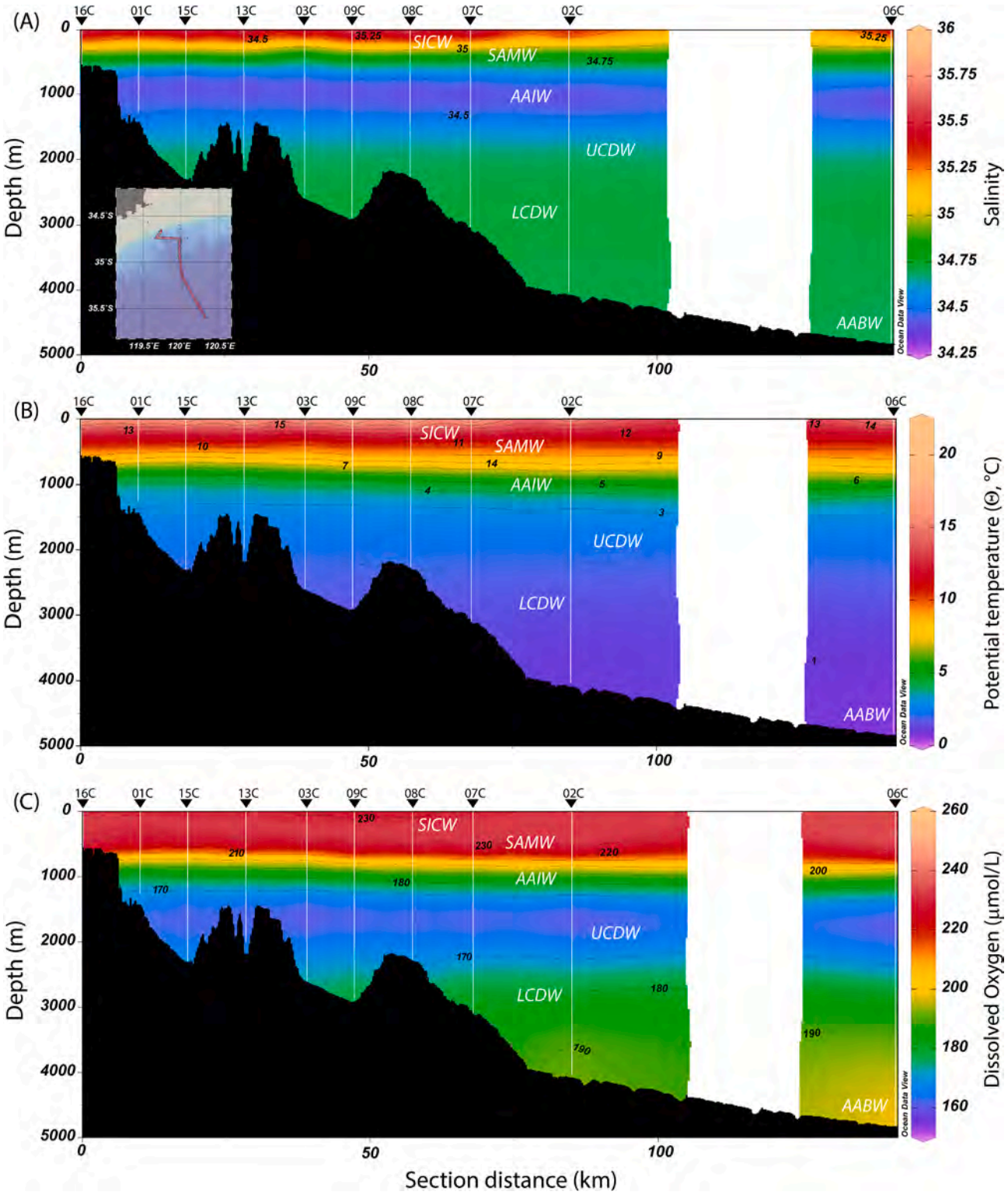

Fig. 7. N-S section of (A) salinity, (B) potential temperature, and (C) dissolved oxygen concentrations from CTD casts deployed at the shelf break (16C) to the open ocean (06C) in the Bremer canyon systems.

(<300 m), the $\delta^{13}C_{DIC}$ continuously decreased through SAMW, AAIW, and UCDW (500–2500 m), starting from a broad, site-specific range of 0.74–1.31 ‰ to a narrower range of 0.55–0.70 ‰ at 2500 m; this decrease was correlated with increasing DIC concentration ($R^2 = 0.62$, $p < 0.001$; Supplementary Figure 7D). Below 2000 m, the $\delta^{13}C_{DIC}$ was relatively constant, at around ~0.70 ‰ (0.55–0.90 ‰) through the lower UCDW, LCDW, and AABW, but the differences between sampling locations (0.25 ‰) were above the analytical uncertainty (0.10 ‰). The surface waters across all sites generally had higher $\delta^{13}C_{DIC} > 1.0$ ‰ in the upper water masses (SICW and SAMW), with values > 1.2 ‰ further offshore (02C and 06C).

The stable hydrogen and oxygen isotope composition of seawater varied between −2.7 and +4.5 ‰ in $\delta^{2}H_{H2O}$ and between −0.34 and +1.42 ‰ in $\delta^{18}O_{H2O}$, while displaying the usual strong correlation ($\delta^{2}H$

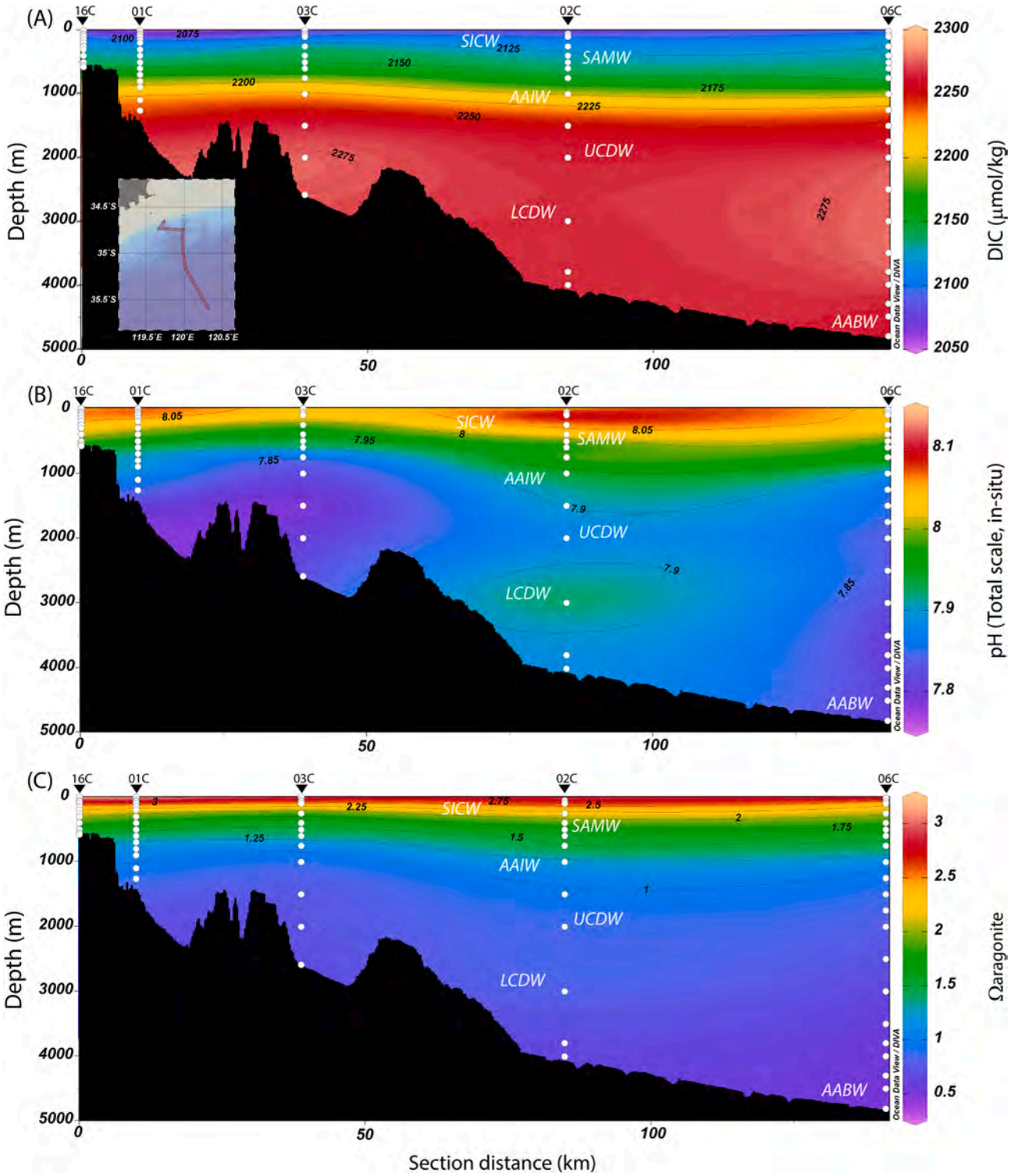

Fig. 8. N-S sections of (A) dissolved inorganic carbon, (B) pH, and (C) aragonite saturation state from CTD casts deployed at the shelf break (16C) to the open ocean (06C) in the Bremer canyon systems.

$= 4.30 \times \delta^{18}O\text{-}0.70$, $R^2 = 0.76$, $p < 0.001$). Both δ^2H_{H2O} and $\delta^{18}O_{H2O}$ were more positive at the surface and decreased across the SICW and SAMW, however, below 800 m these values did not display any further decrease and instead stabilised around 0.8 ‰ for $\delta^{18}O_{H2O}$ and 0.0 ‰ for δ^2H_{H2O} (Supplementary Figure 7B, C, E). Variability was greater for $\delta^{18}O_{H2O}$ compared to δ^2H_{H2O}, and both were higher near shore in shallower waters (01C).

Seawater compositions at the mouth of the PC (19C) have the same depth pattern as the BCS. However, many parameters (TA, DIC, $\delta^{18}O_{H2O}$, δ^2H_{H2O}, Si-SiO_3, P-PO_4, Ba) tend to have values above or in the upper range of those observed around the BCS, particularly for AAIW and partially UCDW water masses. This depth interval also corresponded to the differences observed between the T-salinity and T-DO relationships, with PC waters having higher salinity and lower DO concentrations than those from the Bremer and Hood canyons between temperatures of ~2–5 °C (Fig. 6).

Table 2
Water masses identified in the Bremer canyon systems with key seawater properties. SICW: South Indian Central Water; SAMW: Subantarctic Mode Water; AAIW: Antarctic Intermediate Water; UCDW: Upper Circumpolar Deep Water; LCDW: Lower Circumpolar Deep Water; AABW: Antarctic Bottom Water; σ_θ = potential density; DO = dissolved oxygen; DIC = Dissolved Inorganic Carbon; AOU = Apparent Oxygen Utilization.

Water mass	Depth (m)	Temp. (°C)	Salinity	σ_θ (kg/m^3)	DO (μmol/L)	DIC (μmol/kg)	AOU (μmol/kg)
SICW	~ 0–300	~ 21–11	35.9–34.9	25.1–26.7	~210–250	2059–2138	−5.9–37.7
SAMW	~ 300 to 600–800	~ 11–7.5	34.9–34.6	26.7–27.2	>220	2126–2174	33.6–119.3
AAIW	~ 600–800 to 1200–1400	~ 7.5–3	<34.5	26.8–27.5	210–170	2143–2234	43.7–160.5
UCDW	~ 1200–1400 to 2600	~ 3–2	34.4–34.7	27.4–27.8	<170	2234–2278	146.4–169.9
LCDW	~ 2600–3800	~ 2–1.2	~34.7	27.8	170–190	2264–2280	148.6–155.5
AABW	~ 4100–4800	~ 1	~34.7	27.8	>200	2259–2270	144.5–145.4

5.4. Dive surveys and faunal sampling

5.4.1. General observations

Pelagic, nektic, and demersal organisms encountered encompass cnidarians, annelids, echinoderms, cephalopods, and fish. Jellyfish cnidarians belonging to Scyphozoa (e.g. the holopelagic *Periphylla*, Fig. 9A), Cubozoa, Ctenophora, and Siphonophora (Fig. 9B) were observed. A swimming squid-worm, *Teuthidodrilus*, was sampled in the PC at 1925 m (Fig. 9C). Pelagic holothurians (e.g. *Enypniastes*) were occasionally seen in the Hood and Perth canyons (Fig. 9D, 9O). Various rare deep-sea cephalopods (Fig. 9E-H), such as a *Grimpoteuthis* octopus and *Galiteuthis phyllura* squid, were seen swimming in the water column, a *Pholidoteuthis* (possibly *P. massyae*) squid probed the muddy substrate in the PC, and a *Magnapinna* big-fin squid was recorded above the muddy substrate in the BCS (Knob Canyon, 2998 m). Many species of fish inhabit the canyons at all depths, mainly Actinopterygii and, subordinately, Elasmobranchii. *Bathypterois* (Fig. 9I), *Bathyraja* (Fig. 9J), *Figaro* (Fig. 9K), and the unusual *Chaunax suttkusi* (Fig. 9L) were seen consistently on the deep soft bottoms of the canyons. Orange roughy, eels, toad and coffin fish, grenadiers, cardinal, batfish, anglers (e.g. *Gigantactis*, Fig. 9M), whiptails, sharks, skates were also represented with many others yet to be identified.

Mobile benthos that inhabited the deep, muddy, seafloor was mostly represented by echinoderms, with many species of elasipod holothurians (e.g. *Benthodytes* spp. Fig. 9N) and occasionally pelagic *Enypniastes* feeding on the substrate (Fig. 9O), echinoids, dominantly Echinothuriidae (Fig. 9P-Q) sometimes in aggregations, and asteroids (Fig. 9R). Various annelids including scale worms were also observed. Enteropneustid acorn worms, Torquatoridae (Fig. 10A), were commonly seen actively reworking surface sediments. The brachyuran *Chaceon albus* (Fig. 10B) represented the most conspicuous decapod crawling on muddy bottoms but was equally observed on rocky substrates. Other noticeable crustaceans were hermit crabs (Paguroidea), frequently carrying commensal anemones, and galathaeids. Various molluscs were filmed on soft bottoms, like Octopoda cephalopods (including *Grimpoteuthis*, Fig. 10C) and gastropods. Sessile benthos was mostly represented by cnidarians, sponges, and annelid worms.

Vagrant benthos included various echinoderms, such as cidaroids and mostly echinoids. *Dermechinus* formed aggregations on rocky substrates and atop of cnidarian colonies, especially antipatharians, and often formed large debris fields of post-mortem skeletal hash (Fig. 10D). Crinoids and ophiuroids (Fig. 10E-G) were very common, with occasional fields on top of mounds (Supplementary Figure 8B) but mostly as dense clusters on coral hosts, while holothurians and asteroids were less commonly seen. Many crustacean taxa were present, most obvious were lobsters (Fig. 10H), crabs that included the giant *Pseudocarcinus gigas* (Fig. 10I), and shrimps. Mobile benthic organisms also included worms, gastropods, and rare pycnogonids (Fig. 10J).

Sessile benthos was dominated by cnidarians but also included sponges, molluscs, barnacles, ascidians, bryozoans, serpulid annelids, and brachiopods. Porifera was mostly represented by Demospongiae and, less commonly, Hexactinellid glass sponges (Fig. 10J). While sponges were a ubiquitous but not dominant component of the communities colonising the rocky substrates at all depths explored, Demospongiae together with bryozoans formed dense animal forests at shallower depths in the Hood Canyon (~180–300 m, Fig. 10K). The giant stalked barnacle (Crustacea, Cirripedia), *Smilium*, formed spectacular clusters on black coral colonies (Fig. 10L). In the BCS especially, the bivalve *Acesta* (Fig. 10M), frequently colonised the vertical walls in clusters, and accumulations of dead shells formed carbonate hash deposits. Cnidaria was the most obvious Phylum in the canyons in both diversity and spatial coverage. They formed animal forests, as distinct zoned communities or as collections of mixed fauna that comprised scleractinians, soft and calcified octocorals, black corals, anemones, and hydroids together with other associated taxa (Fig. 10F, 10G, 10L, see also 5.4.2).

The occurrence of a specialised chemosynthetic-based community associated with whale falls in the BCS (Fig. 10O) is another notable discovery. It comprised various chemosymbiotic organisms with a predominance of bathymodioline mussels.

The benthic macro and megafauna differed in composition throughout the surveyed areas (ANOSIM: $p < 0.01$), with hard substrates (from individual rocks to extensive outcrops) hosting far more diverse assemblages ($p < 0.05$, Fig. 11A). See also Supplementary Figures 9–10, cruise report (Trotter et al., 2021), and Data Availability links below.

5.4.2. Deep-water corals

Deep-water corals were found to be the dominant sessile benthic component with their abundance varying with depth (Fig. 11B). The 500–1000 m depth interval hosted the highest number of coral specimens, mainly species with aragonitic (cup corals and other scleractinians) and calcitic (stylasterid, *Corallium*, and bamboo coral) skeletons (Fig. 12). Proteinaceous corals (antipatharians) were more abundant between ~600 and 1400 m water depth. Within the 500–1000 m bathymetric interval, the abundance of corals differed between explored areas ($p < 0.01$).

Live solitary scleractinians were observed and sampled from all three study areas, they are taxonomically diverse, and span the widest geographic and depth ranges (344–2243 m) from the canyon floors to the muddy shallows along the shelf-edge margin (e.g. Fig. 13A, 13E, 13I-L). Those conditions encompass temperatures from 2.2 to 11 °C, salinity from 34.4 to 34.7 units, and dissolved oxygen concentrations between 156 and 243 μmol/L. Live colonials (948–1212 m) seemed common in the BCS but rare around the Mount Gabi seamount (Fig. 13B-D, 13I) and were not observed in the Perth Canyon. Dead and subfossil colonial (670–1532 m) and solitary corals (331–2260 m) were very common at all three study areas, preserved either in-situ on rock surfaces and under overhangs, or within sediment deposits on the substrate; they were especially prolific at Mount Gabi (Fig. 13F-H).

Octocorals, (bamboos and Coralliidae) were common and occasionally collected live from the three study areas (383–2896 m; Fig. 14A-B, 14E, 14G, 15A-C). Antipatharians (Figs. 14J-K, 14 M−N; 15E-F, 15H-I) were also common in the BCS and Leeuwin (sampled from 665 to 1054 m). Large colonies of antipatharians and octocorals typically hosted clusters of echinoderms (baskets stars, brittlestars, and urchins), barnacles, stylasterids, cup corals, bivalves, and squat lobsters (Fig. 15).

Below is an overview of the corals noted within each study area in

Fig. 9. Representative species observed through the water column to the substrate. (A) helmet jelly, *Periphylla*, Knob Canyon, dive 312, 2879 m; (B) siphonophore colony, *Erenna*, Perth Canyon, dive 331, 991 m; (C) squid worm, *Teuthidodrilus*, Perth Canyon, dive 328, 1938 m; (D) pelagic holothurian, *Enypniastes eximia*, Perth Canyon, dive 328, 2235 m; (E) squid, *Pholidoteuthis massyae*, Perth Canyon, dive 331, 897 m; (F) big-fin squid, *Magnapinna*, dive 312, Knob Canyon, 2912 m; (G) cockatoo glass squid, *Galiteuthis phyllura*, Hood Canyon, dive 323, 1020 m; (H) bob-tail squid, Leeuwin scarp, dive 325, 445 m; (I) tripod fish, *Bathypterois*, Perth Canyon, dive 329, 2982 m; (J) skate, *Bathyraja*, Bremer Canyon, dive 322, 652 m; (K) catshark, *Figaro boardmani*, Hood Canyon, dive 320, 362 m; (L) sea toad, *Chaunax suttkusi*, Perth Canyon, dive 330, 550 m; (M) whipnose angler, *Gigantactis*, Knob Canyon, dive 312, 3236 m; (N) elasipod holothurian, *Benthodytes*, Perth Canyon, dive 329, 2641 m; (O) pelagic holothurian feeding on substrate, *Enypniastes*, Perth Canyon, dive 329, 2614 m; (P) echinoid, Perth Canyon, dive 328, 2155 m; (Q) Echinothuriidae echinoid, Perth Canyon, dive 327, 673 m; (R) large asteroid, Knob Canyon, dive 312, 3262 m.

relation to depth, water mass, and substrate. Supplementary Table 2 lists all live corals collected and ambient seawater conditions.

5.4.2.1. Bremer canyon systems. In the deep waters of lower UCDW and LCDW near the mouth of the Henry and Knob canyons (~2500–3300 m), the muddy floor and rocky flanks were colonised by antipatharians (e.g. *Schizopathes, Alternipathes, Umbellapathes*), isidid octocorals (e.g. *Lepidisis, Keratoisis, Acanella*), and small soft corals.

In the western arm of the Hood Canyon, antipatharians (*Stichopathes*), bamboos, and soft corals were observed along the muddy canyon floor and lower flanks within AAIW-UCDW depths (~1190–1550 m). Some live scleractinian cup corals, *Vaughanella* (Fig. 13A), *Polymyces,* and *Caryophyllia*, were found on isolated rocks and walls (collected from ~1485–1535 m) well below the aragonite saturation horizon (~1000 m, see section 3.3.2). Live *Desmophyllum* and *Vaughanella* occurred at similar depths in the eastern head of the Hood

Fig. 10. Representative fauna observed on sediment and rocky substrates. (A) acorn worm feeding on the substrate, Torquatoridae n.sp. (D. Holland, pers, com. Dec. 2020), Perth Canyon, dive 329, 3004 m; (B) brachyuran crab, *Chaceon albus*, Perth Canyon, dive 330, 715 m; (C) Dumbo octopus, *Grimpoteuthis*, Hood Canyon, dive 323, 1109 m; (D) aggregation of cactus urchin, *Dermechinus* and nearby antipatharian, Hood Canyon, dive 314, 706 m; (E) crinoid on fossil coral rubble with ectoparasitic gastropod (arrow) on stem, Mount Gabi, dive 324, 768 m; (F) basket stars (bs), crinoids (cr), and small ophiuroids (op) colonising a large antipatharian (*Trissopathes*?), Hood Canyon, dive 314, 746 m; (G) Gorgonocephalidae basket stars (bs) and crinoid (cr) inhabiting an Isididae, Leeuwin scarp, dive 325, 695 m; (H) Palinurid lobster in sponge-bryozoan forest, Hood Canyon, dive 320, 219 m; (I) giant decapod crab, *Pseudocarcinus gigas* Hood Canyon, dive 320, 212 m; (J) glass sponge *Hyalonema* with zoanthid (z) on stem and a crawling sea-spider (Pycnogonida), Perth Canyon, dive 328, 1856 m; (K) bryozoan-sponge (Demospongiae) forest, Hood Canyon, dive 320, 190 m; (L) giant stalked barnacle, *Smilium* (Sm; A. Hosie, pers. comm.), colonising a large antipatharian (*Leiopathes*), Hood Canyon, dive 314, 773 m; (M) large limid bivalve *Acesta* (Ac) with cup corals (co), Hood Canyon, dive 314, 866 m; (N) anemone (Actinostoloidea), Knob Canyon, dive 312, 3218 m; (O) scattered bones from whale fall with urchin inhabiting skull, Hood Canyon, dive 323, 1111 m. Note laser lights spaced 10 cm apart (green dots in G).

Canyon. Dead and subfossil fragments of scleractinians (*Desmophyllum, Vaughanella, Polymyces, Caryophyllia,* and *Solenosmilia*) were contained within shell hash on the substrate or in-situ on the canyon walls (~950–1530 m) in the western head of the Hood Canyon.

The most abundant and diverse populations of corals (and other calcifiers) were found on hard substrates along the steep rocky walls of the Hood and Bremer canyons (Figs. 11, 12, 16) within the oxygen and nutrient-rich AAIW and SAMW. Dead and live solitary and colonial scleractinian corals were found on exposed cliff faces, under ledges, along crevices, live corals sometimes resettled onto loose rocks or dead

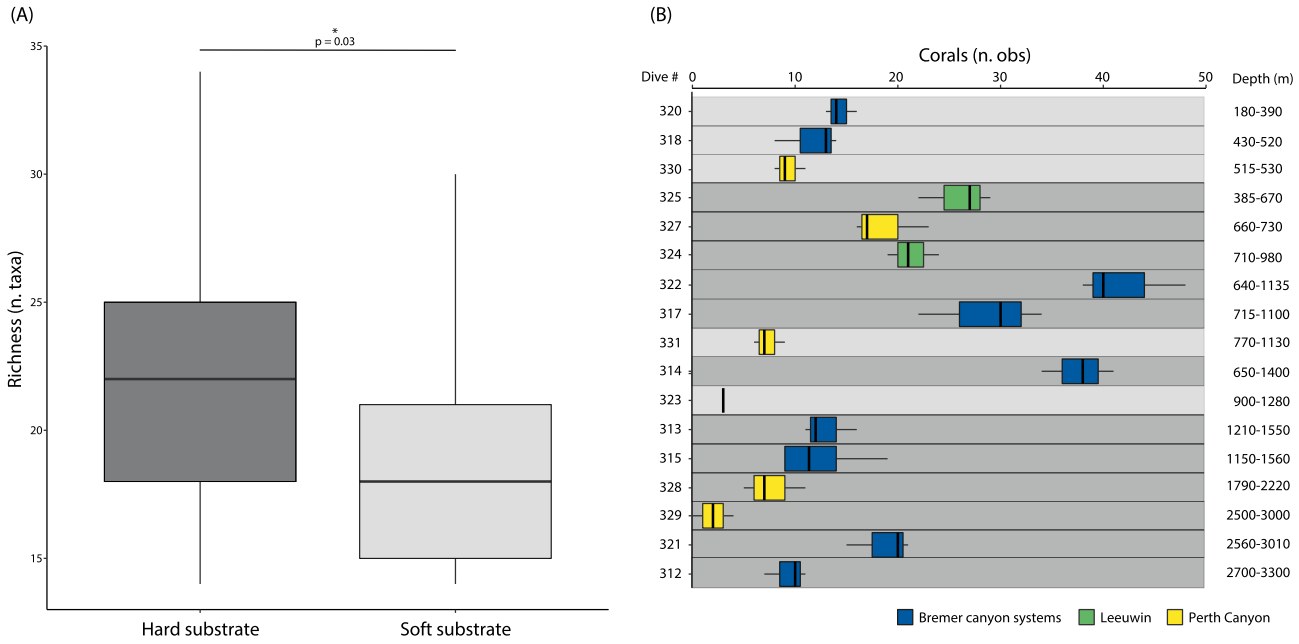

Fig. 11. (A) Boxplot of taxonomic richness (i.e. number of taxa observed) for substrate type with significativity of Kruskal-Wallis test. Boxes extend from the 25th to the 75th percentile with the horizontal line representing median value. The vertical lines indicate the most extreme values within 1.5 interquartile range of the 25th and 75th percentile; (B) boxplot of live coral abundances (number of observations, excluding actinarians) in each dive and ordered by depth.

colonies (Fig. 13B-E). Cup corals were also often found living near the base or on branches of *Corallium*. Live colonial *Solenosmilia* (~948–1229 m) and the solitary corals *Desmophyllum, Javania,* and *Caryophyllia* (~683 and 1229 m) were observed and sampled. Live Coralliidae, bamboos (*Lepisidis, Keratoisis*), and antipatharians (e.g. *Leiopathes, Trissopathes*?, *Bathypathes, Stichopathes*) were also common (703–1385 m) with large colonies typically hosting numerous other species (Figs. 14-15). Small stylasterids and alcyonaceans were commonly observed along the canyon walls, with *Metallorgorgia, Chrysogorgia, Iridogorgia, Paragorgia* (Fig. 14C) and large spectacular *Anthoptilum* pennatulaceans (Fig. 14D, F) occasionally seen. Significant deposits of dead scleractinian debris (solitary and colonial species) and associated shell hash were common in both canyons within SAMW-AAIW depths.

In transitional SAMW-AAIW waters in the eastern head of the Hood Canyon, distinct habitat 'zones' (Fig. 15H-I, 15 K) comprised significant populations of antipatharians (*Bathypathes* and *Plumapathes*) associated with *Dermechinus* (~700 m), and primnoid-dominated *Callogorgia* and especially *Calyptrophora* coral gardens (~660 m).

Within the higher temperatures and oxygen content of SAMW above the Bremer Canyon, live *Caryophyllia* and *Flabellum* colonised the muddy flats (641–678 m). Diverse and relatively abundant populations of solitary corals also inhabited the shallower soft sediments in the Hood Canyon (~340–500 m), represented by *Flabellum*, *Stephanocyathus*, *Caryophyllia* (one small specimen attached to a nylon rope and a small dead black coral), *Cyathotrochus* and *Truncatoflabellum*. Small dead solitary corals were also retrieved from sediment scoops. Occasional bamboos (*Keratoisis, Lepidisis*) colonised some rocky outcrops (~380 m), and primnoid *Callogorgia* inhabited sponge and bryozoan forests (~180 m).

5.4.2.2. Mount Gabi and Leeuwin scarp. The north face of Mount Gabi was surveyed from base (970 m) to top (720 m) through the AAIW. Extensive deposits of recently dead and subfossil scleractinian corals, dominated by *Solenosmilia* and *Desmophyllum*, covered the base of the seamount and much of its entire structure (Fig. 13F-J). Dead and subfossil scleractinians were sometimes attached to branches of dead *Corallium*. Subparallel rows of these deposits were often observed on top of the seamount (Fig. 5M). Live scleractinians (*Desmophyllum Polymyces, Caryophyllia*, and *Solenosmilia;* Fig. 13I-J), antipatharians (*Bathypathes, Stauropathes*: Fig. 14J-K), bamboo coral (*Lepidisis*), pennatulaceans (e.g. *Anthoptilum*) and stylasterids were occasionally seen.

The steep north wall of the continental slope and shallower muddy flats above were explored (~430 and 770 m) within SAMW and AAIW. Most common along the wall were large live colonies of antipatharians (*Leiopathes, Bathypathes*) and branching bamboos (*Keratoisis*), occasional Coralliidae, and the scleractinian *Enallopsammia* (e.g. Fig. 15A, 15D). Small stylasterids were also common. Dead and live octocoral colonies often hosted live cup corals at their bases or on branches. Live cup corals occurred along the slope walls and within soft sediments above the scarp, represented by *Crispatotrochus*, *Caryophyllia*, *Desmophyllum,* isolated patches of very small, slender, specimens of the solitary flabellid *Javania*, with *Flabellum* and *Paraconotrochus* scattered on the shallow muddy flats (489–504 m). Deposits of dead disarticulated bamboo fragments and *Corallium, and* dead/subfossil *Caryophyllia* and *Desmophyllum* were often observed.

5.4.2.3. Perth Canyon. In the deep waters of the LCDW (~2530–3000 m) towards the mouth of the canyon, the only skeletonised corals observed were a few bamboos (*Lepidisis/Keratoisis*, *Acanella*) and various soft corals (e.g. *Callogorgia, Metallorgorgia*; Fig. 14G). In UCDW at the juncture of the two main limbs of the canyon, live solitary scleractinian corals (*Rhombopsammia*, Fig. 13K; *Polymyces, Javania*) were living in the fine sediments to depths of ~2220 m, >1200 m below the aragonite saturation horizon (~1000 m). Live soft corals (e.g. *Chrysogorgia, Iridogorgia, Calyptrophora*; Fig. 14H), antipatharians (e.g. *Bathypathes*), and bamboos (*Lepidisis*) were also observed. Occasional dead/subfossil scleractinians (*Desmophyllum* and *Vaughanella*) occurred within the sediment substrate or in-situ on the canyon wall.

Along the west wall of the canyon's main eastern limb, live solitary cup corals were found living in patches of fine sediments (*Fungiacyathus*) or on occasional hard rock surfaces (*Crispatotrochus* and *Polymyces*) within AAIW depths (~870–1125 m). Dead/subfossil scleractinians, mainly cup corals (*Desmophyllum* and *Polymyces*), were also observed and sampled (~770–920). Antipatharians and bamboo corals were occasionally observed.

On the NE-SW trending scarp at the northernmost site, several

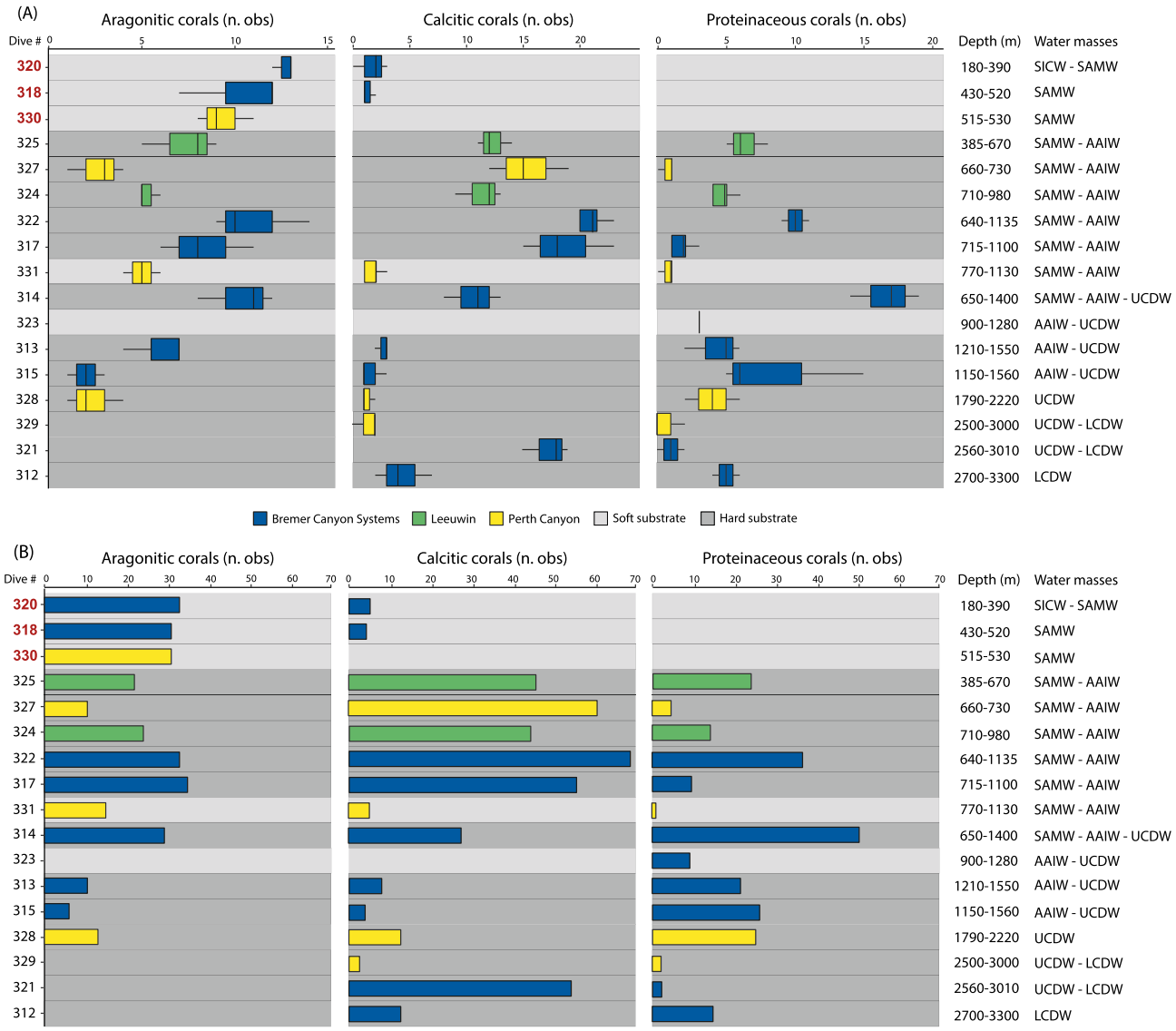

Fig. 12. (A) Boxplot of the number of observations of live aragonitic (scleractinians), calcitic (Stylasterids, bamboo corals and *Corallium*), and proteinaceous corals (antipatharians) in the substransects generated from the original dives showing the trend of distribution of corals by depth. Primnoids were not included since calcified structures are embedded in their proteinaceous matrix. Water masses within coral ranges also shown. Grey bars refer to the main type of substrate on which live corals were observed. Red bold font identifies shallower dives dominated by soft substrates inhabited by semi-infaunal corals. (B) bar chart of total number of live aragonitic, calcitic, and proteinaceous coral observations for each dive, ordered by depth.

terraces but otherwise flat expanses ~10 km from the canyon rim, were explored within upper AAIW to lower SAMW depths (~665 and ~740 m). Slightly northeast of the Last Glacial Maximum fossil coral grounds discovered in 2015 (FK150301, Site F: Trotter et al., 2019), we again encountered extensive subfossil coral deposits dominated by colonial (*Solenosmilia*) and solitary (*Desmophyllum, Polymyces*) subfossil corals, with the occasional subfossil octocoral (*Corallium*). Small live stylasterids were common. Large live colonies of *Paragorgia*, Corallidae, *Bathypathes, Trissopathes*? and *Leiopathes* (675–733 m) were occasionally observed. Live cup corals were often attached to rocks and rubble, especially *Javania* and *Polymyces*.

In the shallower depths of the SAMW (~390 to 715 m) near the head of the canyon, delicate and robust species of small and large solitary corals were found living within the soft silty substrate, including *Flabellum* (Fig. 13L), *Paraconotrochus, Stephanocyathus*, *Fungiacyathus*, *Caryophyllia*, *Letepsammia*, and *Deltocyathus*.

6. Discussion

Here we report the first observations of several large and otherwise unexplored deep water canyon environments along the Southern Ocean-facing margin of Australia's southwest continental shelf. Albeit limited by the area explored compared to the vastness of these systems, the specific focus on coral sampling, and the overall lack of prior knowledge of these habitats, we present some preliminary quantitative analyses of coral community distributions and extensive observations within an environmental context. Our integrated analyses of the physical and chemical oceanography, bathymetry, and geology, together with documentation of their inhabitants including ~160 h of high-resolution video footage, represent a major advancement in our knowledge of these deep-sea communities. They provide the first insights into the canyon habitats within a multi-disciplinary framework and build upon the initial expedition to the PC in the SE Indian Ocean (McCulloch et al., 2016; Trotter et al., 2018, 2019), thereby enabling some of the first in-situ ROV-based comparisons between these SW Australian submarine canyon systems.

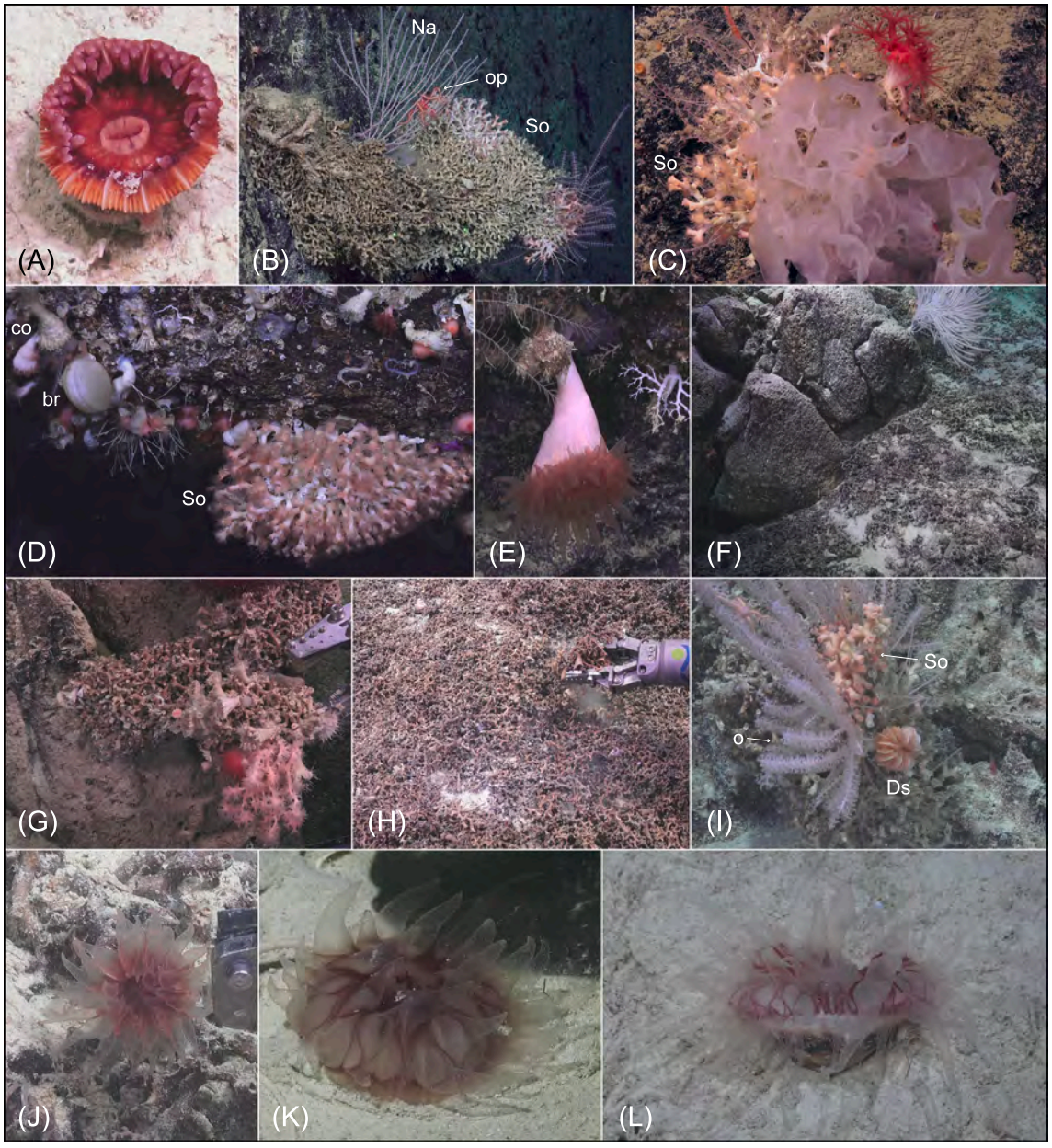

Fig. 13. Images of some live and subfossil deep-sea scleractinian corals observed and/or collected. (A) live *Vaughanella*, Hood Canyon, dive 315, 1532 m; (B) dead and live *Solenosmilia* (So) with associated octocoral *Narella* (Na) and ophiuroids (op), Hood Canyon, dive 314, 983 m; (C) live *Solenosmilia* (So) and sponge, Bremer Canyon, dive 322, 1033 m; (D) live colonial *Solenosmilia* (So), live and dead cup corals (co) and brachiopod (br), Hood Canyon, dive 317, 953 m; (E) live *Javania*, Hood Canyon, dive 317, 757 m; (F-H) fossil coral rubble, base and walls of Mount Gabi, dive 324, 964–822 m; (I) live clump of *Solenosmilia* (So), *Desmophyllum* (Ds), and octocoral (o) on fossil coral substrate, Mount Gabi, dive 324, 952 m; (J) live *Polymyces* on loose fossil coral debris, Mount Gabi, dive 324, 906 m; (K); live micrabaciid coral, *Rhombopsammia*, deepest scleractinian found, Perth Canyon, dive 328, 2219 m; (L) live *Flabellum* with extended polyp, Perth Canyon, dive 330, 550 m. Note laser lights spaced 10 cm apart (green dots in B).

These two canyon systems, the BCS and PC, are similar in being located on a passive margin with no landward connectivity, thus representing sediment-starved systems lacking present-day terrigenous input or structural disturbances. While their geological context is similar, differing structural components influence tributary orientation, with those in the PC following an east–west sinusoidal configuration defined by major fault structures, whereas the dendritic BCS are mostly aligned north–south. Although facing different ocean basins, the waters within both canyon systems are, nevertheless, similar and relatively homogenous (with few exceptions, see below) being dominantly influenced by their proximity to the northward flowing waters emanating from the Southern Ocean.

6.1. Coral distribution

There are several clear similarities in the bathymetric distribution of faunal colonisation across all three of our study sites (BCS, Leeuwin, and PC). In the case of corals, scleractinians and associated fauna favoured depths within the nutrient- and oxygen-rich waters of the AAIW and SAMW (Figs. 11, 12, 16). Taxonomically diverse sediment-dwelling solitary corals colonised the muddy sediments near the shelf-edge margin, with *Flabellum* collected from all three locations; rocky canyon walls accommodated congregations of solitary and colonial scleractinians as well as large colonies of antipatharians and octocorals; and isolated occurrences of small solitary corals lived within the low

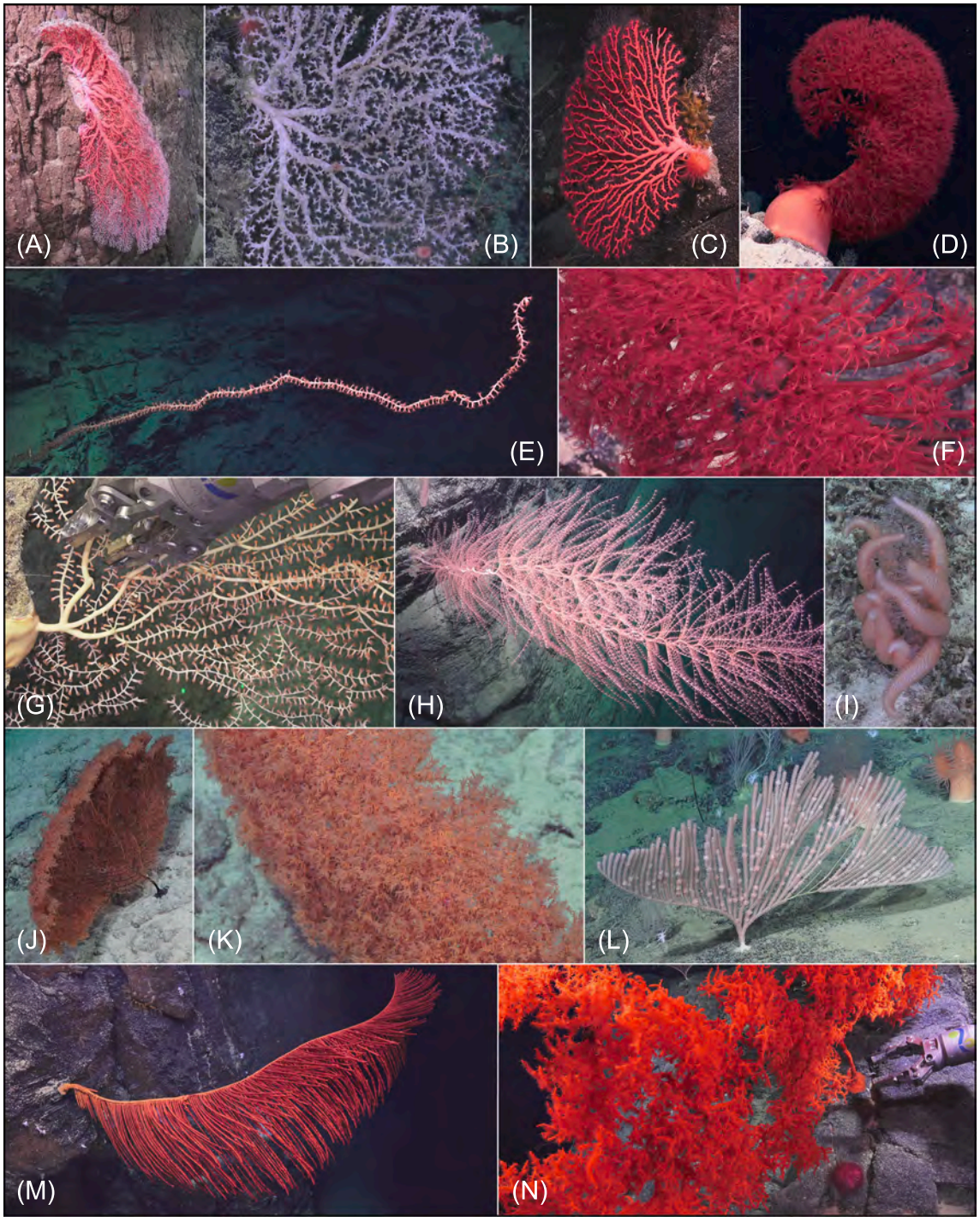

Fig. 14. Various octocorals and antipatharians observed and/or collected. (A) Coralliidae, Perth Canyon, dive 327, 692 m; (B) Coralliidae, Hood Canyon, dive 317, 930 m; (C) *Paragorgia*, Hood Canyon, dive 314, 779 m; (D, F) *Anthoptilum*, Bremer Canyon, dive 322, 872 m; (E) *Lepidisis*?, Hood Canyon, dive 321, 2770 m; (G) Isididae, Perth Canyon, dive 329, 2552 m; (H) *Iridogorgia*, Perth Canyon, dive 328, 1870 m; (I) antipatharian encased in carnivorous asteroid Mount Gabi, dive 324, 768 m; (J-K) *Stauropathes*, Mount Gabi, dive 324, 957 m; (L) *Calyptrophora*, Hood Canyon, dive 314, 676 m; (M) Bathypathes, Bremer Canyon, dive 322, 782 m; (N) *Leiopathes*, Hood Canyon, dive 317, 717 m. Note laser lights spaced 10 cm apart (green dots in G).

oxygen and aragonite undersaturated waters of the UCDW (Fig. 16).

A qualitative presence/absence comparison of major coral types in an environmental context (cf. Taviani et al., 2016; Trotter et al. 2019) shows the general patterns of colonisation described above (Fig. 16). However, within AAIW and lower SAMW, there is an apparent asymmetry of live coral communities across the region (Fig. 11B), being noticeably depauperate in the PC (with no colonial species observed) whereas large aggregations of corals with associated fauna including patches of colonial *Solenosmilia* were commonly encountered across the Southern Ocean-facing BCS. Statistical analyses support field observations that the BCS accommodates a significantly higher number of coral individuals compared to the PC (Supplementary Table 3) where aragonitic ($p < 0.01$) and calcitic ($p < 0.05$) coral abundance is particularly low (Fig. 12). However, we suspect that the actual occurrences are underrepresented by the abundance counts for the BCS especially, not only due to the inherent inaccuracies and difficulties of real-time remote

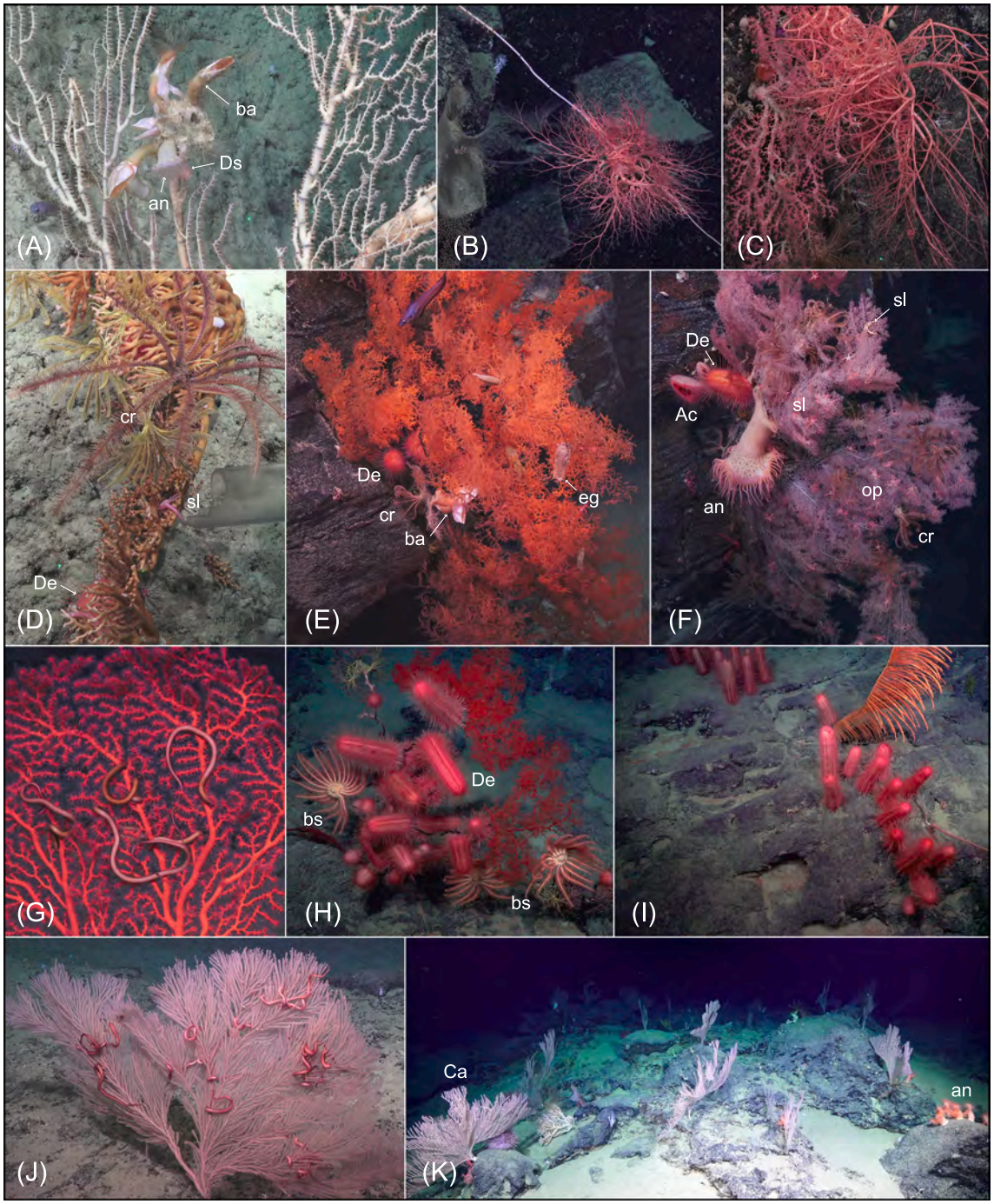

Fig. 15. Faunal associations observed, with mostly live octocorals and antipatharians commonly hosting various taxa. (A) large Isididae colonised by goose barnacles (ba), anemone (an), and *Desmophyllum* cup coral (Ds), Leeuwin scarp, dive 325, 628 m; (B) basket star hanging on an Isididae with tissue absent from much of stem, Hood Canyon, dive 314, 909 m; (C) Coralliidae hosting a basket star, Hood Canyon, dive 314, 881 m; (D) scleractinian *Enallopsammia* colonised by crinoids (cr), *Dermechinus* cactus urchin (De), squat lobsters (sl), Leeuwin scarp, dive 325, 536 m; (E) large *Leiopathes* colony inhabited by numerous taxa including *Dermechinus* urchins (De), crinoids (cr), elasmobranch eggs (eg), barnacles (ba), and fish, Bremer Canyon, dive 322, 755 m; (F) large *Trissopathes*? colonised by various species including large anemones (an), *Dermechinus* cactus urchins (De), crinoids (cr), ophiuroids (op), and squat lobsters (sl), Bremer Canyon, dive 322, 749 m; (G) serpent stars inhabiting *Paragorgia*, Bremer Canyon, dive 322, 704 m; (H) *Leiopathes* hosting *Dermechinus* cactus urchins (De) and brisingid seastars (bs), Hood Canyon, dive 314, 703 m; (I) *Bathypathes* commonly associated with cactus urchins, Hood Canyon, dive 314, 706 m; (J) *Callogorgia* colonised by serpent stars, Bremer Canyon, dive 322, 700 m; (K) coral garden dominated by *Calyptrophora* (ca), Hood Canyon, dive 314, 655 m. Note laser lights spaced 10 cm apart (green dots in A, B, D).

video identifications, but where widespread occurrences were not possible to count.

The striking difference in colonisation between these canyons is likely controlled by a combination of canyon-specific and regional environmental factors (see below). Conversely, representation of sediment-dwelling solitary scleractinians on the flats above the canyons at equivalent depths within shallower SAMW is similar between the canyons (Fig. 12; Supplementary Table 2).

6.2. Faunal associations

In the BCS, faunal associations were especially obvious, often

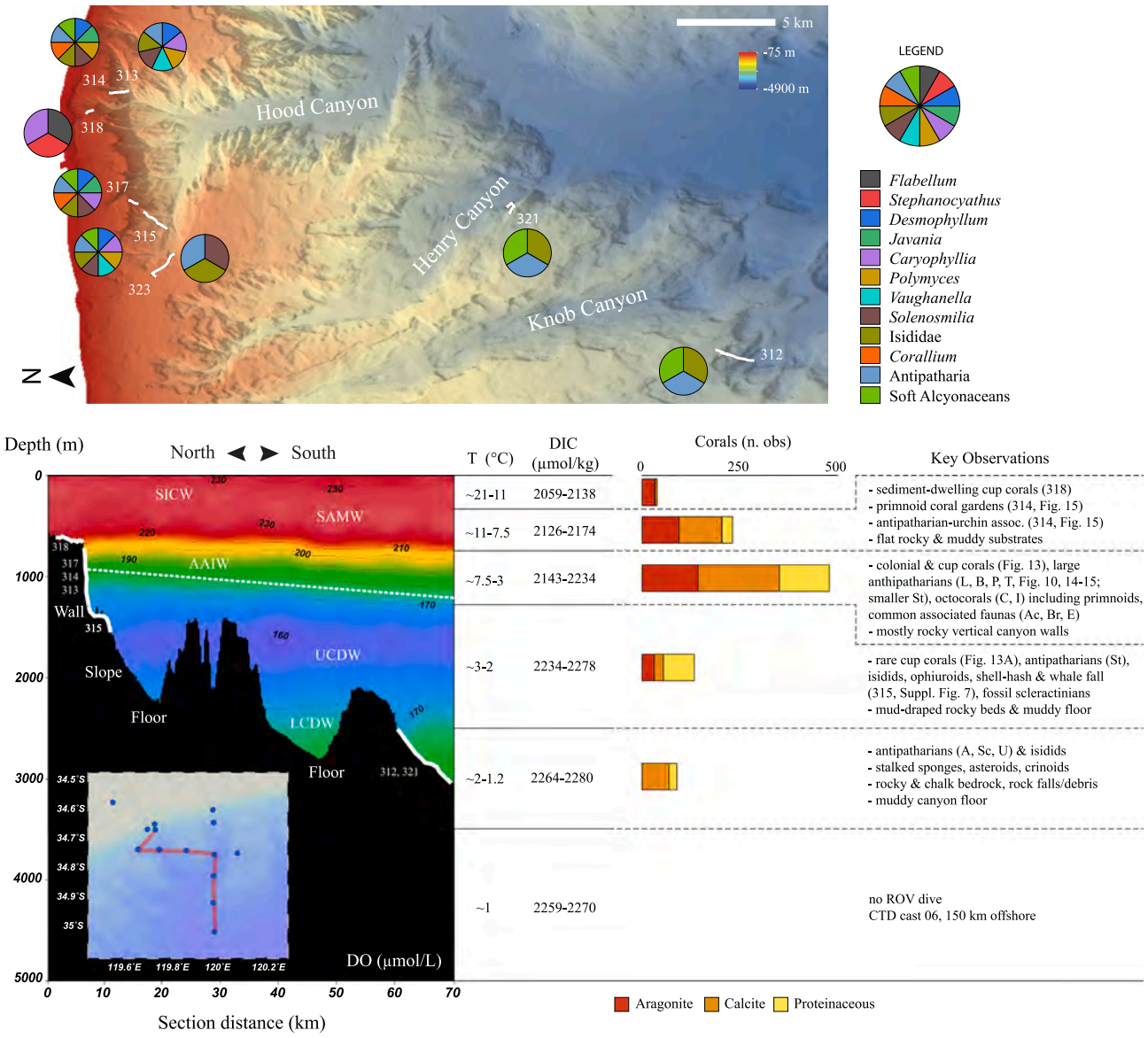

Fig. 16. Generalised representation of environments in the Bremer canyon systems, relating seawater conditions to key substrate and coral communities observed at most ROV dive sites (320 and 322 not shown). (Top) Map showing presence of main cnidarian taxa observed live around the Hood, Henry, and Knob canyons. Sectors of pie charts are not proportional to abundance but provide a qualitative representation of conspicuous taxa at each dive site shown. See Trotter et al. (2019) for similar observations in 2015 from the Perth Canyon during cruise FK150301. (Bottom) Seawater profile showing key water masses with dissolved oxygen concentration contours (µmol/L) based on CTD casts (circles, inset). ROV dive paths (white lines) are located within the seawater transect shown (red line, inset); dotted white line denotes shoaling aragonite saturation horizon. Note that the seawater profile generated was interpolated between CTD casts. General ranges in seawater temperature (T) and dissolved inorganic carbon (DIC) for each water mass (note depths vary depending on site due to northward shoaling), coral abundance (by mineral composition) for all BCS dive sites surveyed, and key substrate and biological observations (Key Observations) within those water masses are summarised. SICW: South Indian Central Water; SAMW: Subantarctic Mode Water; AAIW: Antarctic Intermediate Water; UCDW: Upper Circumpolar Deep Water; LCDW: Lower Circumpolar Deep Water; AABW: Antarctic Bottom Water. Seawater profile generated using Ocean Data View. Antipatharians: A = *Alternipathes*, B = *Bathypathes*, L = *Leiopathes*, P = *Plumapathes*, Sc = *Schizopathes*, St = *Stichopathes*, T = *Trissopathes*, U = *Umbellapathes*; C = *Corallium*; I = Isididae; Ac = *Acesta* bivalve; Br = brachiopod; E = various echinoderms; some dives and figure numbers shown in brackets.

forming large and striking communities. Patches of colonial scleractinians (*Solenosmilia*) provided a substrate for cup corals and other taxa, such as echinoderms, sponges, small octocorals, and bivalves. Branching octocorals (e.g. *Corallium*) and especially large colonies of antipatharians commonly hosted asteroides and ophiuroids, sometimes with many other species (e.g. cactus urchins, crustaceans, solitary corals, anemones, goose barnacles etc), forming hotspots of diverse communities (Fig. 15). Thus, corals appear to be important community centres, either within patches of faunal aggregations along the canyon walls (~700–1200 m in AAIW-SAMW) or forming spectacular animal forests as spatially extensive populations within distinct ecological zones (~650–700 m in SAMW). For example, along the flatter margin at the head of the Hood Canyon, cactus urchins (*Dermechinus*) associated with black corals (*Bathypathes* and *Plumapathes*) were dominant at ~700 m, which transitioned to an interval of coral gardens (~600 m) dominated by primnoid corals (mostly *Calyptrophora*), their branches aligned in the same orientation to capture nutrients from the water column (Fig. 15K; Fig. 16). However, large coral communities were rarely observed in the PC, with occasional antipatharian and octocoral colonies noted (Fig. 14A, G).

6.3. Environmental controls

Various environmental factors can influence the biogeography and colonisation of sessile epibenthos in submarine canyons, specifically the nature of the substrate, local hydrography, and the availability of nutrients (see Roberts et al., 2006; Trincardi et al., 2007; Canals et al. 2009; McLain and Barry, 2010; De Leo et al., 2014; Amaro et al., 2016; Carvalho et al., 2016; Bargain et al., 2018; Chauvet et al., 2018; Ismail et al., 2018; Appah et al., 2020). Analogous arguments apply to infaunal life in canyon habitats (De Leo et al., 2014; Campanyà-Llovet et al., 2018). The greater prevalence of well-lithified exposed rock surfaces and overhangs along the canyon walls of the BCS provide robust attachment surfaces amenable to colonisation by epibenthic organisms (Fig. 16). Notably, all three major coral groups assessed according to their skeletal matrix, aragonite, calcite, and proteinaceous, are most abundant along the steep hard canyon walls within SAMW-AAIW (Figs. 12, 16). Conversely, the softer, friable carbonate lithologies often accompanied by significant dissolution features common in the PC (Trotter et al., 2019) are less secure, a feature not normally associated with canyon walls in systems from other ocean basins where hardgrounds are dominant.

Oceanographic conditions, including oxygen levels, water temperature, and hydrodynamics by which currents enable the transport of nutrients throughout canyon systems, can be highly variable in time and space. Seasonal and inter-annual changes in current flow and water mass interactions can control both nutrient upwelling/downwelling events and oxygenation. The seawater data reported herein thus reflect a brief snapshot in time during Austral summer (February), when the south-flowing sub-surface boundary current (Leeuwin Current) is weaker. The key water masses identified in both the BCS and PC (waters at the Leeuwin sites not measured) are nevertheless consistent with the temperatures, salinity, and dissolved oxygen concentrations reported in regional oceanographic studies (Woo et al., 2006; Woo and Pattiaratchi, 2008; Akhir et al., 2020). Although most parameters measured across our sites are very consistent (Supplementary Figures 2–7, Supplementary Table 1), there are a few notable exceptions between the PC and BCS (Fig. 6): (1) significant mixing of the upper waters (SICW and SAMW) in the BCS shown by highly variable dissolved oxygen, salinity, and carbon isotope seawater compositions; and (2) a marked offset in salinity and especially dissolved oxygen in intermediate and deep waters. Such local differences in canyon conditions likely influence benthic colonisation.

In both canyon systems, megabenthos and especially scleractinians were mostly found along the walls while sediment-dwelling solitary corals inhabited the shallower muddy flats (Fig. 16; BCS ~340–1230 m, and PC ~390–1125 m). Within these depth intervals, temperatures range from 3.1 to 11 °C, salinity ~34.4–34.9, and dissolved oxygen concentrations from 147 to 244 μmol/L, consistent with the wide ranges reported for other deep-water coral sites in canyon systems or carbonate mound structures in the Southern Ocean and other oceanic basins (e.g. Thresher et al., 2014; Glogowski et al., 2015; Hebbeln et al., 2020; Raddatz et al., 2020). The AAIW, UCDW and LCDW in the PC, however, have distinctly lower dissolved oxygen concentrations than the BCS (Fig. 6; DO minimum ~145 μmol/L at 1320 m vs ~160 μmol/L at 1650 m), where the low-oxygen UCDW (defined by the DO minimum) shoals and becomes warmer as it flows northward into the SE Indian Ocean. The shoaling and partial mixing with the overlying AAIW exposes biota inhabiting these and shallower depths in the PC to less oxygenated waters compared to the BCS. Oxygen values as low as 150 μmol/L correspond to 3.35 mL/L, which is close to the minimum oxygen levels typically required for some deep-water coral species, such as the colonial reef-forming *Lophelia pertusa* (presently recognised as *Desmophyllum pertusum*: Addamo et al., 2016), to maintain normal aerobic functions (~3.2 mL/L; Dodds et al., 2007). Conditions in the PC approach this threshold, which might relate to the lack of colonial species (*Solenosmilia*) that are common in the BCS. On the Tasman seamounts off southeast Australia, the oxygen minimum zone (165 μmol/kg = 3.78 mL/L) coincides with lower faunal diversity and a clear gap in the colonisation of both *Desmophyllum* and *Solenosmilia* reefs (Thiagarajan et al., 2013; Thresher et al., 2014). However, coral-based benthic communities off Mauritania, Angola, and Namibia survive, with some flourishing, in extreme environments (Ramos et al., 2017; Hanz et al., 2019; Hebbeln et al., 2020) where the stress of warm and hypoxic conditions are countered by abundant nutrient supply. In the highly productive upwelling systems offshore Angola especially, colonial (*Lophelia*) reefs thrive within ~8–14 °C and oxygen concentrations of ≤ 1 mL/L (Hebbeln et al., 2020).

DIC concentrations at the sites where most of the corals were collected in the BCS and PC (within SAMW and AAIW) range between ~2140 and 2230 μmol/kg (Fig. 16), which are generally higher than the value (2170 μmol/kg) reported by Flögel et al. (2014) as the threshold for the formation of *Lophelia* reefs and mounds covering a large horizontal area and vertical extension (Supplementary Figure 11). Our DIC values are more consistent with conditions encountered in the Coral Mounds off Mauretania (2183–2240 μmol/kg) that are characterized by small and frequently isolated *L. pertusa* colonies.

6.4. Nutrient supply

Nutrient availability is a key controller of some deep-sea biogeography patterns. Interestingly, the dissolved inorganic nutrients (DIC, N-NOx, P-PO_4, Si-SO_3, Ba) measured across our SW Australian sites are very consistent, although surprisingly, concentrations in the more northern PC are slightly higher (or at the upper range) than in the BCS (Supplementary Figures 2–4). This is likely due to the progressive aging of these water masses as they leave their Southern Ocean source and flow northwards. In particular, the aerobic microbial remineralisation of particulate organic matter consumes oxygen and thus increases the apparent oxygen utilization, dissolved inorganic carbon, and nutrient content (Supplementary Table 1). Dissolved inorganic carbon in the upper oceans is regulated primarily by equilibration with atmospheric CO_2, and for the range of temperatures typical for Australian coastal shallow waters (15–25 ℃), $\delta^{13}C_{DIC}$ is expected to be between −0.5 and +1.5 ‰ (Mook et al., 1974). Within the upper water masses of the SAMW and SICW in the BCS, the high variability in $\delta^{13}C$ compositions (~0.6–1.6 ‰, Supplementary Figure 7) reflects differences in productivity and respiration across the different sites, together with different rates of mixing and their exchange with the atmosphere. However, biological inputs are rather minor and considering the observed range, not higher than ± 3 % of total DIC.

The waters around southwest Australia are well-known to be oligotrophic due to the warmer poleward flowing Leeuwin Current transporting low nutrient water of tropical origin. Surface waters are therefore very low in nitrate (Hanson et al., 2005) with concentrations often below the measurement limits of instruments (<0.1 μM). Chlorophyll-*a*, a proxy for primary production, reaches a maximum concentration of ~1 mg/m^3 at 60–80 m in the PC (Rennie et al., 2009a; Trotter et al., 2019) and up to ~1.5 mg/m^3 at 80 m in the BCS (Bouchet et al., 2018; Salgado Kent et al., 2020), deep maxima at depths from 70 to 100 m being a general feature across the southwest region (Hanson et al., 2005, 2007). These chlorophyll concentrations are comparable to those in the western Mediterranean (Bosc et al., 2004) and the Gulf of Mexico (Georgian et al., 2016) but lower than other deep-water coral sites in the North and South Atlantic (e.g. White et al., 2005, Hebbeln et al., 2020). Faunal colonisation in the southwest Australian canyons also share similarities with Mediterranean canyons (e.g. Gori et al., 2013; Fabri et al., 2014; Taviani et al., 2019) where scleractinian corals occur in patches, unlike larger colonial reef-forming colonies common on carbonate mounds in the Atlantic (*Lophelia*) and off Tasmania (*Solenosmilia*).

Given the overall consistency in nutrient depth profiles between the PC and BCS together with the high variability in $\delta^{13}C$ in the upper waters of the BCS, a longer-term and thorough depth-integrated analysis of

productivity and particulate organic matter (used by the corals as a food source) is required to constrain the complex physico-chemical processes occurring in these canyons. An important factor in transporting nutrients to sustain deep-water coral ecosystems is the local hydrodynamic processes operating at various depths (Juva et al., 2020 and references therein), which have a critical influence on biogeography. Internal currents and eddies within the PC drive highly variable and transient fluxes in nutrients and krill abundance, which has been related to transient cetacean populations (Rennie et al., 2009a). Unfortunately, very little is known about currents and tide regimes within the BCS, these processes being known to control food supply, oxygen, and larval dispersal of canyon faunas elsewhere, which are generally considered among the primary drivers of coral distribution (e.g. White et al., 2005; Dullo et al., 2008; Wienberg et al., 2018; Rebesco and Taviani, 2019). The high variability in dissolved oxygen, salinity, and $\delta^{13}C$ within the shallower SICW and SAMW in the BCS suggests significant physical mixing (e.g. eddy-scale) compared to the consistent profiles across the PC (Trotter et al., 2019), implying differences in local hydrodynamics within these systems. Recently, hydrodynamic modelling explored the interaction between slope-confined topography in the Bremer canyon systems and a westward slope current, equivalent to the Flinders Current (Kämpf, 2021). The model suggests that the Hood Canyon especially would induce an upslope flux that concentrated available particulate organic matter onto the upper continental slope, thereby providing a nutrient source for suspension feeders.

Thus, a combination of local, canyon-specific factors likely influences megabenthos colonisation in these canyons, with the BCS inhabitants benefiting from the greater prevalence of robust rocky substrates, comparatively higher dissolved oxygen concentrations, significant upper ocean mixing suggesting enhanced upwelling of nutrients and surface productivity. In addition, the Southern Ocean-facing BCS is directly exposed to more extreme weather conditions emanating from Antarctica, especially during the winter months, which would enhance physical mixing.

6.5. Global context

From a global perspective, these oligotrophic canyon environments off southwest Australia contrast to well-studied submarine canyons of the Northern Hemisphere, which are located within more nutrient-rich boundary current systems. Examples of the latter that sustain important cnidarian populations (among others) are the Whittard Canyon and others in the NE Atlantic (Morris et al., 2013; van den Beld et al., 2017; Robert et al., 2020), NW Atlantic canyons (Etnoyer and Warrenchuk, 2007; Brooke and Ross, 2014; Quattrini et al., 2015), and Barkley Canyon in the NE Pacific (Chauvet et al., 2018; Campanyà-Llovet et al., 2018). In general, very few studies have investigated canyons exposed to oligotrophic waters (e.g. De Leo et al., 2014; Elasar, et al., 2013; Currie and Sorokin, 2014; Conlan et al., 2015; Trotter et al., 2019). Our case-study documents flourishing benthic life, including charismatic deep-water corals in the BCS that are comparable in terms of diversity and density of macrobenthic populations to those canyons located within nutrient-rich settings. As concluded for other canyons (Campanyà-Llovet et al., 2018), we speculate that the combination of substrate conditions (morphology, hydrodynamics), dissolved oxygen, and nutrient availability control the macrobenthos distribution in the southwest Australian canyons. Thus, not only do these canyons experience at least transient nutrient peaks becoming seasonal hotspots of marine life, including large cetacean populations (Pattiaratchi, 2007; Rennie et al., 2009a; Salgado Kent et al., 2020), we now show that the Southern Ocean-facing BCS also supports significant coral-based communities. Although representing the first snapshots of these environments, they nevertheless contribute rare, new data on deep-sea habitats from oligotrophic canyon systems, which adds a new perspective to the global view of submarine canyon environments (Fernandez-Arcaya et al., 2017; De Leo and Puig, 2018; Matos et al., 2018).

6.6. Fossil occurrences and implications for paleobiogeography

In a broader temporal context, the fossil deposits of both solitary (e.g. *Desmophyllum*) and colonial (*Solenosmilia*) corals at all three sites is a significant discovery (Trotter et al., 2021), which provides insights into the favourability of coral colonisation over longer timescales across this region. The large coral deposits found in the northern most site in the PC, at Mount Gabi, and in the Bremer canyon systems, reveal that such communities had flourished in the past, being regionally widespread across southwest Australia. The sheer abundance and expanse of sub-fossil corals discovered between ~700 and 1000 m at Mount Gabi is particularly extraordinary, where in-situ specimens covered exposed rock, and massive rubble deposits were piled around the base, on ledges along walls, and on top of the ~300 m high seamount (Figs. 5M, 13F-H). This contrasts to the very sporadic, impoverished occurrences of living scleractinian corals observed today. The questions remain, however, whether coral deposits are also prolific around other faces of Mount Gabi and if dead coral is an inherent structural component of the rock matrix. Resolving these requires more ROV surveys and a targeted geological programme to sample drill cores and associated rocks from in and around the seamount.

These fossil deposits build significantly on our previous discovery of coral graveyards in the PC of Last Glacial Maximum age (Trotter et al., 2019; Trotter et al., 2022), with the new PC finds revealing the greater areal extent of their occurrence beyond that reported previously around this site. Reconnaissance uranium-series analyses of the fossil corals collected at the three study areas reveal a wide age range (~180 to ~1 ka), but mostly span the last glacial period (~11 to 35 ka) at both Mount Gabi and the Perth Canyon, with the BCS coral ages mostly <5 ka (Trotter et al., 2021). Whether the prolific coral deposits at Mount Gabi were built up gradually over millennia or this region was once a major coral hotspot is unclear and requires further sampling and analyses. However, the virtually continuous deposits along the entire ROV traverse (2665 m) seems consistent with a potential hotspot scenario rather than localized occurrences associated with skeletal accumulations over time. The predominance of LGM ages from the Mount Gabi deposits at least implies that significant coral communities flourished throughout this period. Notably, the expansion of *Solenosmilia* mounds and reefs during glacial periods have been noted off Brazil (Raddatz et al., 2020) and south of Tasmania (Fallon et al., 2014). High resolution uranium-series dating together with a suite of geochemical proxy analyses are ongoing to determine what oceanographic changes occurred at these sites during different periods that likely controlled the waxing and waning of deep-water corals and their present distribution.

7. Additional noteworthy observations

There are several additional noteworthy discoveries:

(1) We observed various solitary corals (*Vaughanella*, *Polymyces*, *Caryophyllia*, *Desmophyllum*, and *Rhombopsammia*) between depths of 1420–2220 m in the BCS and PC, thus well below the aragonite saturation horizon (Supplementary Figure 6A). The aragonite saturation horizon (ASH, i.e. the depth where Ω is equal to 1) varies from ~1500 m in the open ocean (02C) to ~850 m in the Bremer Canyon (03C) hence shoals towards the continental shelf (Supplementary Figure 6). The ASH in the PC is at ~1000 m depth. Waters below these depths are undersaturated with respect to aragonite, so the majority of scleractinians were observed above the ASH. Sporadic occurrences of cup corals occurring below the ASH were previously noted from the PC (Trotter et al., 2019) and Tasman seamounts (Thresher et al., 2011). This indicates that these species up-regulate their internal saturation state to precipitate their aragonite skeleton in corrosive waters (McCulloch et al., 2012), with their organic tissues

likely protecting their skeletons from dissolution (Ries et al., 2009; Rodolfo-Metalpa et al., 2011).

(2) Along the walls of the scarp north of the Leeuwin Canyon (dive 325), rare live colonial scleractinians represented by *Enallopsammia* were observed only in one location (a large thick-branched colony with several smaller specimens nearby), whereas *Solenosmilia* were commonly recorded throughout the BCS. This apparent mismatch in scleractinian colonisation between these study sites might be due to steep cliff faces often covered by fine sediments, and seemingly fewer rock overhangs along the Leeuwin scarp compared to the BCS, these features potentially less amenable for the growth of more fragile branching colonies. However, our limited observations of these habitats around the Leeuwin site might not be representative given that exploration and sampling during dive 325 was restricted by strong currents, and poor weather precluded additional dives.

(3) Strong current action was also indicated along the top of Mount Gabi, by the often sub-parallel alignment of subfossil deposits that occurred post-mortem, many of these deposits covered with manganese coatings indicating they are relatively old (Fig. 5M).

(4) The finding of *Acesta* is of special ecological and biogeographic interest. This almost cosmopolitan large-size limid colonises precipitous topographies in the deep sea (López Correa et al., 2005; Walz et al., 2014; Gagnon et al., 2015), including canyon habitats, and are often associated with corals (Johnson et al., 2013; Taviani et al., 2019). The *Acesta* discovered in the south-western Australian canyons (also Trotter et al., 2019) may prove to be new to science; furthermore, its shell with clear growth increments is of prime significance for geochemical studies (López Correa et al., 2005).

(5) A *Magnapinna* squid was recorded in the BCS (dive 312). This oceanic cephalopod equipped with plurimetric tentacles was identified for the first time only two decades ago (Vecchione and Young, 1998). Only a few global sightings have been reported to date, the first and only prior recording in Australian waters being further east in 2015 (Osterhage et al., 2020).

(6) Echinoderms were commonly observed perched on bamboo corals with significant portions of coral tissue often stripped from their stems and branches (Fig. 15B). Echinoderms (e.g. cactus urchins, basket stars, and ophiuroids) also conspicuously inhabited antipatharians, often ladened with multiple large specimens. It is not known if this is predatory behaviour.

8. Conclusions

We have provided the first descriptions and analyses of deep-sea habitats in the previously unexplored Bremer canyon systems, Mount Gabi seamount and nearby slope-shelf margin, and new data from the Perth Canyon. Of particular note is the degree of mixing in the upper ocean around the Bremer sites, the comparatively lower dissolved oxygen concentrations in the Perth Canyon in UCDW and AAIW, solitary scleractinians living in aragonite undersaturated waters, spectacular animal forests in the Bremer canyon systems, and subfossil coral deposits across all study areas that are particularly extensive at Mount Gabi and on the Perth Canyon shelf. Furthermore, the new footage undoubtedly contributes the first depictions of new species and/or those rarely sighted globally.

These rare and complementary data sets provide a very important baseline for future deep-sea environmental and biological studies around these canyon and continental shelf-slope areas, which are directly influenced by ocean–atmosphere dynamics occurring within the broader Southern Ocean region. Our novel combination of datasets, especially from around the newly explored Leeuwin and Bremer canyon systems, importantly provide a Southern Ocean perspective on the relationship between seawater properties and faunal gradients, together with the value of submarine canyons and seamounts as potential hotspots of biodiversity in the deep sea.

Thorough examination of the samples collected and extensive ROV footage by various specialists is in progress, which will ultimately provide a more nuanced and quantitatively robust ecological analysis. The prime objective of the cruise, however, was the collection of live (mineralised) and fossil corals, which underpin a large geochemical analytical programme aimed at understanding the environmental controls on deep-sea biogeography and long-term temporal changes in ocean-climate dynamics within the globally significant Southern Ocean region.

We also emphasise that the total area surveyed and imaged constitutes only a very small fraction of these large canyon systems, which highlights the importance of ongoing research into these poorly studied deep-sea habitats.

Declaration of Competing Interest

The authors declare that they have no known competing financial interests or personal relationships that could have appeared to influence the work reported in this paper.

Data availability

Video footage, navigation data, processed multi-beam data, seawater data, faunal tables and ROV logs, as well as cruise reports can be found in the cruise repository on the Schmidt Ocean Institute website: https://schmidtocean.org/cruise/coralandcanyonadventure/#data.

Seawater data can also be found at the URL below, sponsored by the Australia Ocean Data Network: https://catalogue.aodn.org.au//geonetwork/srv/eng/metadata.show?uuid=e8769cd6-8693-4252-8a5e-1ab2a25d4e4e.

Faunas, rocks, and sediments collected during the cruise have been archived by The University of Western Australia (UWA) and the Western Australian Museum (WAM). Samples collected specifically for geochemical analysis reside with the cruise Chief Scientist, Dr Julie Trotter, at UWA (julie.trotter@uwa.edu.au).

Acknowledgments

The authors gratefully acknowledge the Schmidt Ocean Institute for providing R/V *Falkor* and all necessary equipment and crew that enabled us to undertake cruise FK200126. *Falkor's* Captain, (Peter Reynolds) and crew, and the ROV *SuBastian* pilots (Russell Coffield, Kris Ingram, Cody Peyres, Jason Rodriguez, and Adam Wetmore) are thanked for their expert assistance during the cruise. University students and field technicians (Todd Bond, Carlin Bowyer, Jill Brouwer, Paula Cartwright, Sara Hajabane, Kaycee Handley, Netra Sagar, and Taylor Simpkins) are acknowledged for their assistance during and/or after the cruise. We thank officers from the Western Australian Museum (Andrew Hosie, Ana Hara), for their participation during the cruise and some taxonomic identifications. We also thank Tina Molodstova and Asako Matsumoto for assistance with some coral identifications. This work was supported by research funding from the Australian Research Council to JT (FT160100259) and MM, JT, MT, PM (DP21012896), as well as the Italian National Programme of Antarctic Research (PNRA16-00069 Graceful Project) to PM and MT. This research was partly conducted in the Bremer Marine Park and Perth Canyon Marine Park under permit number PA2019-00080-1(2), issued by the Director of National Parks, Australia. The views expressed in this publication do not necessarily represent the views of the Director of National Parks or the Australian Government. This is ISMAR-CNR, Bologna scientific contribution n. 2036.

Appendix A. Supplementary material

Supplementary data to this article can be found online at https://doi.org/10.1016/j.pocean.2022.102904.

References

Addamo, A.M., Vertino, A., Stolarski, J., García-Jiménez, R., Taviani, M., Machordom, A., 2016. Merging scleractinian genera: the overwhelming genetic similarity between solitary *Desmophyllum* and colonial *Lophelia*. BMC Evol. Biol. 16, 108. https://doi.org/10.1186/s12862-016-0654-8.

Akhir, M.F., Pattiaratchi, C.B., Meuleners, M., 2020. Dynamics and seasonality of the Leeuwin current and the surrounding counter-current system in the region south of Western Australia. J. Mar. Sci. Engineer. 8, 552. https://doi.org/10.3390/jmse8080552.

Amaro, T., Huvenne, V.A.I., Allcock, A.L., Aslam, T., Davies, J.S., Danovaro, R., De Stigter, H.C., Duineveld, G.C.A., Gambi, C., Gooday, A.J., Gunton, L.M., Hall, R., Howell, K.L., Ingels, J., Kiriakoulakis, K., Kershaw, C.E., Lavaleye, M.S.S., Robert, K., Stewart, H., Van Rooij, D., White, M., Wilson, A.M., 2016. The Whittard Canyon – A case study of submarine canyon processes. Progr. Ocean. 146, 38–57.

Appah, J.K.M., Lim, A., Harris, K., O'Riordan, R., O'Reilly, L., Wheeler, A.J., 2020. Are non-reef habitats as important to benthic diversity and composition as coral reef and rubble habitats in submarine canyons? Analysis of controls on benthic megafauna distribution in the Porcupine Bank Canyon, NE Atlantic. Front. Mar. Sci. 7 https://doi.org/10.3389/fmars.2020.571820.

Bargain, A., Foglini, F., Pairaud, I., Bonaldo, D., Carniel, S., Angeletti, L., Taviani, M., Rochette, S., Fabri, M.C., 2018. Predictive habitat modeling in two Mediterranean canyons including hydrodynamic variables. Progr. Ocean. 169, 151–168.

Blevin, J., and Cathro, D. (2008). Australian southern margin synthesis: Internal Geoscience Australia Report Compiled by FrOGTech GA707, pp. 104.

Bosc, E., Bricaud, A., Antoine, D., 2004. Seasonal and interannual variability in algal biomass and primary production in the Mediterranean Sea, as derived from 4 years of SeaWiFS observations. Glob. Biogeochem. Cycles 18 (1).

Bouchet, P. J., Meeuwig, J. J., Erbe, C., Salgado Kent, C. P., Wellard, R., and Pattiaratchi, C. B. (2018). Bremer Canyon Emerging Priorities Project EP2: Final Report. National Environmental Science Programme, Marine Biodiversity Hub. University of Western Australia, 32 p.

Bradshaw, B. E., Rollet, N., Totterdell, J. M., and Borissova, I. (2003). A revised structural framework for frontier basins on the southern and southwestern Australian continental margin. Geoscience Australia, Record 2003/03.

Brooke, S., Ross, S.W., 2014. First observations of the cold-water coral *Lophelia pertusa* in mid-Atlantic canyons of the USA. Deep-Sea Res. II 104, 245–251. https://doi.org/10.1016/j.dsr2.2013.06.011.

Campanyà-Llovet, N., Snelgrove, P.V.R., De Leo, F.C., 2018. Food quantity and quality in Barkley Canyon (NE Pacific) and its influence on macroinfaunal community structure. Progr. Oceanogr. 169, 106–119.

Canals, M., Danovaro, R., Heussner, S., Lykousis, V., Puig, P., Trincardi, F., Calafat, A.M., de Madron, X.D., Palanques, A., Sanchez-Vidal, A., 2009. Cascades in Mediterranean submarine grand canyons. Oceanography. 22 (1), 26–43.

Carvalho, F., Kohut, J., Oliver, M.J., Sherrell, R.M., Schofield, O., 2016. Mixing and phytoplankton dynamics in a submarine canyon in the West Antarctic Peninsula. J. Geophys. Res. Oceans 121, 5069–5083. https://doi.org/10.1002/2016JC011650.

Chauvet, P., Metaxas, A., Hay, A.E., Matabos, M., 2018. Annual and seasonal dynamics of deep-sea megafaunal epibenthic communities in Barkley Canyon (British Columbia, Canada): A response to climatology, surface productivity and benthic boundary layer variation. Progr. Ocean. 169, 89–105.

Comeau, S., Edmunds, P.J., Lantz, C.A., Carpenter, R.C., 2017. Seawater carbon chemistry and net primary production and net calcification in coral reef communities. PANGAEA. https://doi.org/10.1594/PANGAEA.878281.

Conlan, K.E., Currie, D.R., Dittmann, S., Sorokin, S.J., Hendrycks, E.d., Orejas, C., 2015. Macrofaunal patterns in and around du Couedic and Bonney submarine canyons. PLoS ONE 10 (11), e0143921.

Coplen, T.B., 1996. New guidelines for reporting stable hydrogen, carbon, and oxygen isotope-ratio data. Geochim. Cosmochim Acta 60 (17), 3359–3360.

Cordes, E.E., Cunha, M.R., Galeron, J., Mora, C., Olu-Le Roy, K., Sibuet, M., Van Gaever, S., Vanreusel, A., Levin, L.A., 2010. The influence of geological, geochemical, and biogenic habitat heterogeneity on seep biodiversity. Mar. Ecol. 31, 51–65. https://doi.org/10.1111/j.1439-0485.2009.00334.x.

Cresswell, G., Peterson, J., 1993. The Leeuwin current south of Western Australia. Mar. Freshw. Res. 44 (2), 285–303. https://doi.org/10.1071/MF9930285.

Currie, D.R., Sorokin, S.J., 2014. Megabenthic biodiversity in two contrasting submarine canyons on Australia's southern continental margin. Mar. Biol. Res. 10 (2), 97–110. https://doi.org/10.1080/17451000.2013.797586.

De Leo, F.C., Puig, P., 2018. Bridging the gap between the shallow and deep oceans: The key role of submarine canyons. Progr. Ocean. 169, 1–5.

De Leo, F.C., Vetter, E.W., Smith, C.R., Rowden, A.A., McGranaghan, M., 2014. Spatial scale-dependent habitat heterogeneity influences submarine canyon macrofaunal abundance and diversity off the Main and Northwest Hawaiian Islands. Deep-Sea Res. 1 (104), 267–290.

Dickson, A.G., 1990. Thermodynamics of the dissociation of boric acid in synthetic seawater from 273.15 to 318.15 K. Deep-Sea Res. I 37, 755–766. https://doi.org/10.1016/0198-0149(90)90004-F.

Dickson, A.G., Afghan, J.D., Anderson, G.C., 2003. Reference materials for oceanic CO_2 analysis: A method for the certification of total alkalinity. *Mar. Chemistry* 80 (2-3), 185–197.

Dickson, A. G., Sabine, C. L., Christian, J.R. Eds. 2007. Guide to Best Practices for Ocean CO_2 Measurements. *PICES* Special Publication 3, 191 pp.

Dodds, L.A., Roberts, J.M., Taylor, A.C., Marubini, F., 2007. Metabolic tolerance of the cold-water coral *Lophelia pertusa* (Scleractinia) to temperature and dissolved oxygen change. J. Exper. Mar. Biol. Ecol. 349 (2), 205–214.

Dullo, W.C., Flögel, S., Rüggeberg, A., 2008. Cold-water coral growth in relation to the hydrography of the Celtic and Nordic European continental margin. Mar. Ecol. Prog. Ser. 371, 165–176.

Duran, E.R., Phillips, H.E., Furue, R., Spence, P., Bindoff, N.L., 2020. Southern Australia Current System based on a gridded hydrography and a high-resolution model. Progr. Ocean. 181, 102254.

Elasar, M., Kerem, D., Angel, D., Steindler, L., Herut, B., Shoham-Frider, E., Barnes, O., Almogi, A., 2013. Akhziv Submarine Canyon: an oasis in the warming oligotrophic Levantine Basin? 40th CIESM Congress, Marseille. Rapp. Comm. int. Mer Médit. 40, 2013.

Etnoyer, P., Warrenchuk, J., 2007. A catshark nursery in a deep gorgonian field in the Mississippi Canyon, Gulf of Mexico. Bull. Mar. Sci. 81, 553–559.

Fabri, M.C., Pedel, L., Beuck, L., Galgani, F., Hebbeln, D., Freiwald, A., 2014. Megafauna of vulnerable marine ecosystems in French Mediterranean submarine canyons: spatial distribution and anthropogenic impacts. Deep-Sea Res. II. 104, 184–207.

Fallon, S.J., Thresher, R.E., Adkins, J., 2014. Age and growth of the cold-water scleractinian *Solenosmilia variabilis* and its reef on SW Pacific seamounts. Coral Reefs 33 (1), 31–38.

Fernandez-Arcaya, U., Ramirez-Llodra, E., Aguzzi, J., Allcock, A.L., Davies, J.S., Dissanayake, A., Harris, P., Howell, K., Huvenne, V.A.I., Macmillan-Lawler, M., Martín, J., Menot, L., Nizinski, M., Puig, P., Rowden, A.A., Sanchez, F., Van den Beld, I.M.J., 2017. Ecological role of submarine canyons and need for canyon conservation: a review. Front. Mar. Sci. 4, 5. https://doi.org/10.3389/fmars.2017.00005.

Fine, R.A., 1993. Circulation of Antarctic Intermediate Water in the South Indian Ocean. Deep Sea Res. 40 (10), 2021–2042.

Flögel, S., Dullo, W.-C., Pfannkuche, O., Kiriakoulakis, K., Rüggeberg, A., 2014. Geochemical and physical constraints for the occurrence of living cold-water corals. Deep-Sea Res. II 99, 19–26. https://doi.org/10.1016/j.dsr2.2013.06.006.

Gagnon, J-M-. Kenchington, E., Port, A., Anstey, L. J., and Murillo, F. J. 2015. Morphological and genetic variation in North Atlantic giant file clams, *Acesta* spp. (Bivalvia: Limidae), with description of a new cryptic species in the north-west Atlantic. *Zootaxa* 4007 (2), 151–180.

Georgian, S.E., DeLeo, D., Durkin, A., Gomez, C.E., Kurman, M., Lunden, J.J., Cordes, E. E., 2016. Oceanographic patterns and carbonate chemistry in the vicinity of cold-water coral reefs in the Gulf of Mexico: Implications for resilience in a changing ocean. Limnol Oceanogr 61 (2), 648–665.

Gibbons, A. D., Barckhausen, U., van den Bogaard, P., Hoernle, K., Werner, R., Whittaker, J.M., Müller, R.D. 2012. Constraining the Jurassic extent of Greater India: tectonic evolution of the West Australian margin, Geochem. Geophys. Geosyst. 13, Q05W13, 25 pp.

Glogowski, S., Dullo, W.-C., Feldens, P., Liebetrau, V., von Reumont, J., Hühnerbach, V., Krastel, S., Wynn, R.B., Flögel, S., 2015. The Eugen Seibold coral mounds offshore western Morocco: oceanographic and bathymetric boundary conditions of a newly discovered cold-water coral province. Geo-Mar. Lett. 35 (4), 257–269.

Gori, A., Orejas, C., Madurell, T., Bramanti, L., Martins, M., Quintanilla, E., Marti-Puig, P., Lo Iacono, C., Puig, P., Requena, S., Greenacre, M., Gili, J.M., 2013. Bathymetrical distribution and size structure of cold-water coral populations in the Cap de Creus and Lacaze-Duthiers canyons (northwestern Mediterranean). Biogeosciences 10 (3), 2049–2060.

Hall, L.S., Gibbons, A.D., Bernardel, G., Whittaker, J.M., Nicholson, C., Rollet, N., Müller, R.D., 2013. Structural Architecture of Australia's Southwest Continental Margin and Implications for Early Cretaceous Basin Evolution. West Australian Basins Symposium.

Hanson, C.E., Pattiaratchi, C.B., Waite, A.M., 2005. Seasonal production regimes off south-western Australia: influence of the Capes and Leeuwin currents on phytoplankton dynamics. Mar. Freshw. Res. 56, 1011–1026.

Hanson, C.E., Pesant, S., Waite, A.M., Pattiaratchi, C.B., 2007. Assessing the magnitude and significance of deep chlorophyll maxima of the coastal eastern Indian Ocean. Deep-Sea Res. II. 54 (8-10), 884–901.

Hanz, U., Wienberg, C., Hebbeln, D., Duineveld, G., Lavaleye, M., Juva, K., Dullo, W.-C., Freiwald, A., Tamborrino, L., Reichart, G.-J., Flögel, S., Mienis, F., 2019. Environmental factors influencing benthic communities in the oxygen minimum zones on the Angolan and Namibian margins. Biogeosciences 16, 4337–4356. https://doi.org/10.5194/bg-16-4337-2019.

Heap, A.D., Edwards, J., Fountain, L., Spinnocia, M., Hughes, M., Mathews, E., Griffin, J., Borissova, I., Blevin, J., Mitchell, C., Krassay, A., 2008. Geomorphology, Sedimentology, and Stratigraphy of Submarine Canyons on the SW Australian Slope. Geoscience Australia, Canberra, ACT.

Heap, A.D., Harris, P.T., 2008. Geomorphology of the Australian margin and adjacent seafloor. Aust. Jour. Earth Sci. 55 (4), 555–585. https://doi.org/10.1080/08120090801888669.

Hebbeln, D., Wienberg, C., Dullo, W.-C., Freiwald, A., Mienis, F., Orejas, C., Titschack, J., 2020. Cold-water coral reefs thriving under hypoxia. Coral Reefs 39, 853–859. https://doi.org/10.1007/s00338-020-01934-6.

Huang, Z., Nichol, S.L., Harris, P.T., Caley, M.J., 2014. Classification of submarine canyons of the Australian continental margin. Mar. Geol. 357 (Suppl. C), 362–383. https://doi.org/10.1016/j.margeo.2014.07.007.

Ismail, K., Huvenne, V., Robert, K., 2018. Quantifying spatial heterogeneity in submarine canyons. Progr. Oceanogr. 169, 181–198.
Johnson, M.P., White, M., Wilson, A., Würzberg, L., Schwabe, E., Folch, H., Allcock, A.L., Roberts, J.M., 2013. A vertical wall dominated by *Acesta excavata* and *Neopycnodonte zibrowii*, part of an undersampled group of deep-sea habitats. PLoS ONE 8 (11), e79917.
Juva, K., Flögel, S., Karstensen, J., Linke, P., and Dullo, W-C. 2020. Tidal dynamics control on cold-water coral growth: A high-resolution multivariable study on Eastern Atlantic cold-water coral sites. Front. Mar. Sci. doi.org/10.3389/fmars.2020.00132.
Kämpf, J., 2007. On the magnitude of upwelling fluxes in shelf-break canyons. Cont. Shelf Res. 27, 2211–2223. https://doi.org/10.1016/j.csr.2007.05.010.
Kämpf, J., 2021. Modelling of physical drivers of a large feeding aggregation of killer whales (*Orcinus* orca) in the western Great Australian Bight, Australia. Deep-Sea Res. Part I 171. https://doi.org/10.1016/j.dsr.2021.103526.
Laufkötter, C., Gruber, N., 2018. Will marine productivity wane? Science 359 (6380), 1103–1104.
Laufkötter, C., Vogt, M., Gruber, N., Aumont, O., Bopp, L., Doney, S.C., Dunne, J.P., Hauck, J., John, J.G., Lima, I.D., Seferian, R., Völker, C., 2016. Projected decreases in future marine export production: the role of the carbon flux through the upper ocean ecosystem. Biogeosciences 13 (13), 4023–4047.
Lee, K., Kim, T.-W., Byrne, R.H., Millero, F.J., Feely, R.A., Liu, Y.-M., 2010. The universal ratio of boron to chlorinity for the North Pacific and North Atlantic oceans. Geochim. Cosmochim Acta 74 (6), 1801–1811.
López Correa, M., Freiwald, A., Hall-Spencer, J., and Taviani, M. 2005. Distribution and habitats of Acesta excavata (Bivalvia: Limidae) with new data on its shell ultrastructure, in eds. Freiwald, A. and Roberts, J. M., Cold-water corals and ecosystems, 173–205, Springer Berlin Heidelberg.
Lueker, T.J., Dickson, A.G., Keeling, C.D., 2000. Ocean pCO_2 calculated from dissolved inorganic carbon, alkalinity, and equations for K_1 and K_2: validation based on laboratory measurements of CO_2 in gas and seawater at equilibrium. Mar. Chem 70 (1-3), 105–119.
MacIntosh, H., Althaus, F., Williams, A., Tanner, J.E., Alderslade, P., Ahyong, S.T., Bax, N., Criscione, F., Crowther, A.L., Farrelly, C.A., Finn, J.K., Goudie, L., Gowlett-Holmes, K., Hosie, A.M., Kupriyanova, E., Mah, C., McCallum, A.W., Merrin, K.L., Miskelly, A., Mitchell, M.L., Molodtsova, T., Murray, A., O'Hara, T.D., O'Loughlin, P. M., Paxton, H., Reid, A.L., Sorokin, S.J., Staples, D., Walker-Smith, G., Whitfield, E., Wilson, R.S., 2018. Invertebrate diversity in the deep Great Australian Bight (200–5000 m). Mar. Biodiv. Rec. 11, 23. https://doi.org/10.1186/s41200-018-0158-x.
Matos, F.L., Ross, S.W., Huvenne, V.A.I., Davies, J.S., Cunha, M.R., 2018. Canyons pride and prejudice: Exploring the submarine canyon research landscape, a history of geographic and thematic bias. Progr. Ocean. 169, 6–19.
McCartney, M. S. 1977. Subantarctic Mode Water, in ed. Angel M., A voyage of discovery: George Deacon 70th anniversary, Supplement to Deep Sea Res., 103-119, Pergamon Press, Oxford, New York.
McCulloch M., T., Trotter J. A, Montagna P., Falter J., Dunbar R., and Freiwald A., Försterra, G., López Correa, M., Maier, M., Rüggeberg, A., Taviani, M. et al. 2012. Boron isotope systematics of cold-water scleractinian corals: internal pH up-regulation and response to ocean acidification. Geochim. Cosmochim. Acta 87, 21–34.
McCulloch, M., Trotter, J., Falter, J., Pattiaratchi, C., Montagna, P., Taviani, M., Thresher, R., Hosie, A., Garcia-Corral, L., Haig, D., Foglini, F., Agusti, S., Duarte, C. et al. 2016. ROV Exploration of the Perth Canyon and Assessing the Vulnerability of Deep-sea corals to Climate Change and Ocean Acidification. Schmidt Ocean Institute Cruise FK150301 Final Report. schmidtocean.org/ cruise/perth-canyon-first-deep-exploration/.
McLain, C.R., Barry, J.P., 2010. Habitat heterogeneity, disturbance, and productivity work in concert to regulate biodiversity in deep submarine canyons. Ecology 91, 964–976. https://doi.org/10.1890/09-0087.1.
Middleton, J.F., Bye, J.A.T., 2007. A review of the shelf-slope circulation along Australia's southern shelves: Cape Leeuwin to Portland. Progr. Oceanogr. 75 (1), 1–41. https://doi.org/10.1016/j.pocean.2007.07.001.
Molinelli, E.J., 1981. The Antarctic influence on Antarctic intermediate water. J. Mar. Res. 39, 267–293.
Mook, W.G., Bommerson, J.C., Staverman, W.H., 1974. Carbon isotope fractionation between dissolved bicarbonate and gaseous carbon dioxide. Earth. Planet. Sci. Lett. 22 (2), 169–176.
Morris, K.J., Tyler, R.A., Masson, D.G., Huvenne, V.I.A., Rogers, A., 2013. Distribution of cold-water corals in the Whittard Canyon, NE Atlantic Ocean. *Deep-Sea Res. II* 92, 136–144. https://doi.org/10.1016/j.dsr2.2013.03.036.
Norvick M.S. 2004. Tectonic and stratigraphic history of the Perth Basin, Geoscience Australia Record, 2004/16.
O'Hara, T.D., Williams, A., Ahyong, S.T., Alderslade, P., Alvestad, T., Bray, D., Burghardt, I., Budaeva, N., Criscione, F., Crowther, A.L., Ekins, M., Eléaume, M., Farrelly, C.A., Finn, J.K., Georgieva, M.N., Graham, A., Gomon, M., Gowlett-Holmes, K., Gunton, L.M., Hallan, A., Hosie, A.M., Hutchings, P., Kise, H., Köhler, F., Konsgrud, J.A., Kupriyanova, E., Lu, C.C., Mackenzie, M., Mah, C., MacIntosh, H., Merrin, K.L., Miskelly, A., Mitchell, M.L., Moore, K., Murray, A., O'Loughlin, P.M., Paxton, H., Pogonoski, J.J., Staples, D., Watson, J.E., Wilson, R.S., Zhang, J., Bax, N. J., 2020. The lower bathyal and abyssal seafloor fauna of eastern Australia. Mar. Biodiv. Rec. 13 (1) https://doi.org/10.1186/s41200-020-00194-1.
Osterhage, D., MacIntosh, H., Althaus, F., Ross, A., 2020. Multiple observations of Bigfin Squid (*Magnapinna* sp.) in the Great Australian Bight reveal distribution patterns, morphological characteristics, and rarely seen behaviour. PLoS ONE 15 (11), e0241066.
Pattiaratchi, C. B. 2007. Understanding areas of high productivity within the south-west marine region. Report prepared for the Department of the Environment, Water, Heritage and the Arts. SESE report no. 243, School of Environmental Systems Engineering, the University of Western Australia.
Paul, D., Skrzypek, G., 2006. Flushing time and storage effects on the accuracy and precision of carbon and oxygen isotope ratios of sample using the GasBench II technique. Rapid Commun. Mass Spectrom. 20, 2033–2040.
Quattrini, A.M., Nizinski, M.S., Chaytor, J.D., Demopoulos, A.W.J., Roark, E.B., France, S.C., Moore, J.A., Heyl, T., Auster, P.J., Kinlan, B., Ruppel, C., Elliott, K.P., Kennedy, B.R.C., Lobecker, E., Skarke, A., Shank, T.M., Bianchi, C.N., 2015. Exploration of the canyon-incised continental margin of the northeastern United States reveals dynamic habitats and diverse communities. PLoS ONE 10 (10), e0139904.
R Core Team, 2019. R: A Language and Environment for Statistical Computing. R Foundation for Statistical Computing, Vienna, Austria.
Raddatz, J., Titschack, J., Frank, N., Freiwald, A., Conforti, A., Osborne, A., Skornitzke, S., Stiller, W., Rüggeberg, A., Voigt, S., Albuquerque, A.L.S., Vertino, A., Schröder-Ritzrau, A., Bahr, A., 2020. *Solenosmilia variabilis*-bearing cold-water coral mounds off Brazil. Coral Reefs 39, 69–83. https://doi.org/10.1007/s00338-019-01882-w.
Ramos, A., Sanz, J. L., Ramil, F., Agudo, L. M., and Presas-Navarro, C. 2017 The giant cold-water coral mounds barrier off Mauritania. In: Deep-sea ecosystems off Mauritania: Research of marine biodiversity and habitats in the northwest African margin. Ramos, A., Ramil, F., Sanz, J. L. eds. Springer, Netherlands, Dordrecht, pp 481–525.
Rebesco, M., and Taviani, M. 2019. A turbulent story: Mediterranean contourites and cold-water corals. in Mediterranean Cold-Water Corals: Past, Present and Future, Orejas Saco del Valle C, Jiménez C eds., Springer series: Coral Reefs of the World. Springer, pp. 34-46.
Rennie, S., Hanson, C.E., McCauley, R.D., Pattiaratchi, C., Burton, C., Bannister, J., Jenner, C., Jenner, M.-N., 2009a. Physical properties and processes in the Perth Canyon, Western Australia: links to water column production and seasonal pygmy blue whale abundance. J. Mar. Syst. 77 (1-2), 21–44.
Rennie, S.J., Pattiaratchi, C.B., McCauley, R.D., 2009b. Numerical simulation of the circulation within the Perth submarine canyon, Western Australia. Continent. Shelf Res. 29 (16), 2020–2036.
Ridgway, K.R., Condie, S.A., 2004. The 5500-km-long boundary flow off western and southern Australia. J. Geophys. Res. 109, C04017. https://doi.org/10.1029/2003JC001921.
Ries, J.B., Cohen, A.L., McCorkle, D.C., 2009. Marine calcifiers exhibit mixed responses to CO_2-induced ocean acidification. Geology 37 (12), 1131–1134.
Robert, K., Jones, D.O.B., Georgiopoulou, A., Huvenne, V.A.I., Burns, K.C., 2020. Cold-water coral assemblages on vertical walls from the Northeast Atlantic. Divers. Distribut. 26 (3), 284–298.
Roberts, J.M., Wheeler, A.J., Freiwald, André, 2006. Reefs of the Deep: The Biology and Geology of Cold-Water Coral Ecosystems. Science 312 (5773), 543–547.
Rodolfo-Metalpa, R., Houlbrèque, F., Tambutté, É., Boisson, F., Baggini, C., Patti, F.P., Jeffree, R., Fine, M., Foggo, A., Gattuso, J.-P., Hall-Spencer, J.M., 2011. Coral and mollusc resistance to ocean acidification adversely affected by warming. Nat. Clim. Change 1 (6), 308–312.
Rollet, N., Pfahl, M., Jones, A.., Kennard, J.., Nicholson, C., Grosjean, E., Mantle, D., Jorgensen, D., Bernardel, G., Kempton, R., Langhi, L., Zhang, Y., Hall, L., Hackney, R., Johnston, S., Boreham, C., Robertson, D., Petkovic, P., Lech, M. 2013. Northern extension of active petroleum systems in the offshore Perth Basin - an integrated stratigraphic, geochemical, geomechanical and seepage study, In: Keep, M. and Moss, S. J. (Eds.), The Sedimentary Basins of Western Australia IV. Perth, W.A.: Proceedings of the Petroleum Exploration Society of Australia Symposium, 39 pp.
Salgado Kent, C., Bouchet, P., Wellard, R., Parnum, I., Fouda, L., and Erbe, C. 2020. Seasonal productivity drives aggregations of killer whales and other cetaceans over submarine canyons of the Bremer Sub-Basin, south-western Australia. Aust. Mammal. doi.org/10.1071/AM19058.
Sarmiento, J.L., Gruber, N., Brzezinski, M.A., Dunne, J.P., 2004. High-latitude controls of thermocline nutrients and low latitude biological productivity. Nature 427 (6969), 56–60.
Schlitzer, R., 2020. Ocean Data View, ver. 5.3.0. https://odv.awi.de.
Skrzypek, G., 2013. Normalization procedures and reference material selection in stable HCNOS isotope analyses – an overview. Anal. Bioanal. Chem. 405 (9), 2815–2823.
Skrzypek, G., Ford, D., 2014. Stable isotope analyses of saline water samples on a cavity ring-down spectroscopy instrument. Environ.l Sci Techn. 48, 2827–2834.
Sloyan, B.M., Rintoul, S.R., 2001. The Southern Ocean Limb of the Global Deep Overturning Circulation. J. Phys. Oceanog. 31, 143–173. https://doi.org/10.1175/1520-0485(2001)031/3C0143:TSOLOT/3E2.0.CO;2.
Taviani, M., Angeletti, L., Beuck, L., Campiani, E., Canese, S., Foglini, F., Freiwald, A., Montagna, P., Trincardi, F., 2016. Reprint of 'On and off the beaten track: Megafaunal sessile life and Adriatic cascading processes'. Mar. Geol. 375, 146–160.
Taviani, M., Angeletti, L., Cardone, F., Montagna, P., Danovaro, R., 2019. A unique and threatened deep water coral-bivalve biotope new to the Mediterranean Sea offshore the Naples megalopolis. Sci. Rep. 9, 1–12. https://doi.org/10.1016/j.dsr2.2015.12.008.
Thiagarajan, N., Gerlach, D., Roberts, M.L., Burke, A., McNichol, A., Jenkins, W.J., Subhas, A.V., Thresher, R.E., Adkins, J.F., 2013. Movement of deep-sea coral populations on climatic timescales. Paleoceanography 28, 227–236. https://doi.org/10.1002/palo.20023, 2013.
Thresher, R., Althaus, F., Adkins, J., Gowlett-Holmes, K., Alderslade, P., Dowdney, J.o., Cho, W., Gagnon, A., Staples, D., McEnnulty, F., Williams, A., Bailey, D.M., 2014.

Strong Depth-Related Zonation of Megabenthos on a Rocky Continental Margin (~700–4000 m) off Southern Tasmania. Australia. *PLoS ONE* 9 (1), e85872.

Thresher, R.E., Tilbrook, B., Fallon, S., Wilson, N.C., Adkins, J., 2011. Effects of chronic low carbonate saturation levels on the distribution, growth and skeletal chemistry of deep-sea corals and other seamount megabenthos. Mar. Ecol. Prog. Ser. 442, 87–99. https://doi.org/10.3354/meps0.

Tomczak, M., Liefrink, S., 2005. Interannual variations of water mass volumes in the Southern Ocean. J. Atmosp. Ocean Sci. 10, 31–42. https://doi.org/10.1080/17417530500062838.

Totterdell, J., and Bradshaw, B. 2004. The structural framework and tectonic evolution of the Bight Basin, Eastern Australasian Basins Symposium II. Petroleum Exploration Society of Australia, Special Publication, pp. 41-61, refhub.elsevier.com/S0012-8252(18)30362-3/rf0690.

Totterdell, J.M., Blevin, J.E., Struckmeyer, H.I.M., Bradshaw, B.E., Colwell, J.B., Kennard, J.M., 2000. A new sequence framework for the Great Australian Bight: Starting with a clean slate. APPEA J. 40 (1), 95–118. https://doi.org/10.1071/AJ99007.

Trincardi, F., Foglini, F., Verdicchio, G., Asioli, A., Correggiari, A., Minisini, D., Piva, A., Remia, A., Ridente, D., Taviani, M., 2007. The impact of cascading currents on the Bari Canyon System, SW-Adriatic Margin (Central Mediterranean). Mar. Geol. 246 (2-4), 208–230.

Trotter, J., Montagna, P., Taviani, M., Sadekov, A., Skrzypek, G., Foglini, F., Mazzoli, C., Remia, A., Hosie, A., Hara, A., Pattiaratchi, C., McCulloch, M., 2021. ROV exploration of deep-water coral habitats of southwest Australian submarine canyons. SOI Cruise FK200126 Final. Report. 61, pp.

Trotter, J.A., Pattiaratchi, C., Montagna, P., Taviani, M., Falter, J., Thresher, R., Hosie, A., Haig, D., Foglini, F., Hua, Q., McCulloch, M.T., 2018. Unveiling the Perth Canyon and its deep-water faunas. Biogeosciences Discuss. https://doi.org/10.5194/bg-2018-319.

Trotter, J.A., Pattiaratchi, C., Montagna, P., Taviani, M., Falter, J., Thresher, R., Hosie, A., Haig, D., Foglini, F., Hua, Q., McCulloch, M.T., 2019. First ROV exploration of the Perth Canyon: canyon setting, faunal observations, and anthropogenic impacts. Front. Mar. Sci. 6 (173), 1–24. https://doi.org/10.3389/fmars.2019.00173.

Trotter, J.A., McCulloch, M.T., D'Olivo, J.P., Scott, P., Tisnérat-Laborde, N., Taviani, M., Montagna, P., 2022. Deep-water coral records of glacial and recent ocean-atmosphere dynamics from the Perth Canyon in the southeast Indian Ocean. Quat. Sci. Adv. 6, 100052 https://doi.org/10.1016/j.qsa.2022.100052.

van den Beld, I.M.J., Bourillet, J.-F., Arnaud-Haond, S., de Chambure, L., Davies, J.S., Guillaumont, B., Olu, K., Menot, L., 2017. Cold-water coral habitats in submarine canyons of the Bay of Biscay. Front. Mar. Sci. 4, 118. https://doi.org/10.3389/fmars.2017. 00118.

van Heuven, S. M. A. C., Pierrot, D., Lewis, E., Wallace, D. W. R. 2011. MATLAB Program Developed for CO2 System Calculations, ORNL/CDIAC-105b, Carbon Dioxide Information 10 Analysis Center, Oak Ridge National Laboratory, US Department of Energy, Oak Ridge, Tennessee, doi:10.3334/CDIAC/otg.CO2SYS MATLAB v1.1.

Vecchione, M., Young, R.E., 1998. The Magnapinnidae, a newly discovered family of oceanic squids (Cephalopoda; Oegopsida). S. Afr. J. Mar. Sci. 20, 429–437.

Walz, K.R., Clague, D.A., Barry, J.P., Vrijenhoek, R.C., 2014. First records and range extensions for two *Acesta* clam species (Bivalvia: Limidae) in the Gulf of California. Mexico. *Mar. Biodiv. Rec.* 7 (e60), 1–6. https://doi.org/10.1017/S1755267214000165.

White, M., Mohn, C., de Stigter, H., Mottram, G., 2005. Deep-water coral development as a function of hydrodynamics and surface productivity around the submarine banks of the Rockall Trough, NE Atlantic. In: Freiwald, A., Roberts, J.M. (Eds.), Cold-Water Corals and Ecosystems. Springer Verlag, Berlin, pp. 503–514.

Whittaker, J.M., Williams, S.E., Müller, R.D., 2013. Revised tectonic evolution of the eastern Indian Ocean. Geochem. Geophys. Geosyst. 14, 1891–1909. https://doi.org/10.1002/ggge.20120.

Wienberg, C., Titschack, J., Freiwald, A., Frank, N., Lundälv, T., Taviani, M., Beuck, L., Schröder-Ritzrau, A., Krengel, T., Hebbeln, D., 2018. The giant Mauritanian cold-water coral mound province: Oxygen control on coral mound formation. Quat. Sci. Rev. 185, 135–152. https://doi.org/10.1016/j.quascirev.2018.02.012.

Wijeratne, E.M.S., Pattiaratchi, C.B., Proctor, R., 2018. Estimates of surface and subsurface boundary current transport around Australia. J. Geophys. Res. 123, 3444–3466. https://doi.org/10.1029/2017JC013221.

Williams, S.E., Whittaker, J.M., Halpin, J.A., Müller, R.D., 2019. Australian-Antarctic break up and seafloor spreading: Balancing geological and geophysical constraints. Earth Sci. Rev. 188, 41–58. https://doi.org/10.1016/j.earscirev.2018.10.011.

Wong, A.P.S., 2005. Subantarctic mode water and Antarctic intermediate water in the south Indian Ocean based on profiling float data 2000–2004. J. Mar. Res. 63, 789–812. https://doi.org/10.1357/0022240054663196.

Woo, M., Pattiaratchi, C., 2008. Hydrography and water masses off the Western Australian coast. *Deep-Sea Res. I* 55, 1090–1104. https://doi.org/10.1016/j.dsr.2008.05.005.

Woo, M., Pattiaratchi, C.B., Feng, M., 2006. Hydrography and water masses in the south-eastern Indian Ocean. Unpubl. Report prepared for the Strategic Research Fund for the Marine Environment. CSIRO. School of Environmental Systems Engineering, the University of Western Australia.